The spatial, temporal and volumetric analysis of a large mud volcano province within the Eastern Mediterranean

Christopher Kirkham [a*], Joe Cartwright [a], Christian Hermanrud [b], Christopher Jebsen [c]

[a] Department of Earth Sciences, University of Oxford, South Parks Road, Oxford, UK

[b] Statoil ASA, N-7005 Trondheim, Norway

[c] Statoil, N4032 Stavanger, Norway

** Corresponding author*

E-mail address:chriskirkham6@outlook.com (C. Kirkham)

Abstract

This paper documents and describes through the use of 3D seismic data a prolific mud volcano province within the Eastern Mediterranean. As many as 386 mud volcanoes were mapped within the post-salt succession of the western slope of the Nile Cone, offshore Egypt, using high resolution 3D seismic data. The mud volcanoes within this field display significant geometrical variability in diameter (c. 550 m to c. 5660 m), height (c. 25m to c. 510 m) and volume (c. 0.1 km^3 to c. 3.3 km^3) and lie at depths ranging from c. > 6000 m subsea to c. 3100 m at the seafloor. A close spatial relationship between mud volcanoes and base-salt depressions and regions of anomalous thinning within the immediate pre-salt succession, combined with documented core samples taken from mud volcanoes within this region present a powerful argument for a pre-salt source of mud. 3D seismic interpretation and volumetric analysis of these mud volcanoes and their source region permit the definition and quantification of their depletion zones. A conceptual model for a dynamic liquefaction and sediment withdrawal

process is proposed whereby mud is fed into a central conduit as the depletion zone propagates radially and episodically outwards resulting in a the formation of a concentric depletion zones. Prolonged mud volcanism within this region over the last ~5.3 Ma implies the potential for long lived pre-salt overpressure and continued mud volcanism following the catastrophic hydrodynamic impact of the Messinian Salinity Crisis. It is suggested that the scale of mud volcanism means that this region should be considered as among the largest mud volcano provinces in the world.

Keywords: Mud volcanism; Fluid flow; Overpressure; Liquefaction; Depletion zone; Evaporites; Messinian Salinity Crisis

1 Introduction

Large mud volcano provinces are increasingly recognised as genetically distinct, well defined regions with a prolific flux of mud to the surface over discrete periods of geological time and where hundreds of mud volcanoes have been mapped (Kholodov, 2002; Milkov, 2000). Good examples of such regions include the central Caspian Sea and adjacent areas of Azerbaijan, the Makran, and Trinidad and the Barbados ridge (Kopf, 2002). The central Caspian/onshore Azerbaijan province is a good example, with over 250 significant mud volcano edifices identified to date (Bagirov et al., 1996; Jakubov et al., 1971; Soloviev and Ginsburg, 1994). Equally impressive is the suite of over 450 mud volcanoes that have been interpreted along the Barbados Ridge (Kopf, 2002; Brown and Westbrook, 1988). These large mud volcano provinces have a common geological context: they are located within generally convergent tectonic settings characterised by high sedimentation rates suggesting that a combination of these factors promotes the

development of highly overpressured source regions to provide the necessary driving energy for the extrusional process (Kopf, 2002; Loncke et al., 2004; Milkov, 2000).

In this paper we report a large mud volcano province of previously unrecognised extent from the western margin of the giant Nile Deep Sea Fan (NDSF) (Fig. 1). Surface mud volcanism has been recognised in this area before in numerous studies in the past decade largely from marine geophysical data acquired on research cruises. These recent mud volcanoes form part of a regionally extensive phase of mud volcanism within the Eastern Mediterranean Sea, particularly on the Mediterranean Ridge and the NDSF (Kopf, 2002; Kopf et al., 2001; Kopf and Behrmann, 2000; Mascle et al., 2006; Dupré et al., 2010; Loncke et al., 2004; Dupré et al., 2014; Mascle et al., 2014; Pierre et al., 2014) (Fig. 1). More than 150 mud volcanoes and also pockmarks have been documented specifically in the region of the NDSF within the Egyptian passive margin (Loncke et al., 2004), but these observations were restricted to mud volcanoes at the present day seafloor, observable via near-bottom investigation techniques and swath acoustic data (Loncke et al., 2004). Other buried mud volcanoes have been previously identified particularly within the western province, however the extent of their interpretation has until now been restricted to few seismic profiles that have primarily focused on the Menes Caldera rather than the wider western NDSF region (Dupré et al., 2014; Mascle et al., 2014). The Mediterranean Ridge > 300 km to the northwest represents a neighbouring region of prevalent mud volcanism that contrasts to the Egyptian passive margin, in that the mud volcanoes have formed within the tectono-sedimentary accretionary prism of the Africa-Eurasia subduction zone and are often spatially associated with thrust faults (Mascle et al., 2014; Robertson, 1996). The mud volcanoes offshore Egypt within this study represent a separate specific case governed by different mechanisms that will be explored within this paper.

Our study is based primarily on the interpretation of a large 3D seismic survey over this area, and has allowed the recognition and mapping of several hundred buried mud volcanoes to substantially augment the inventory of those previously identified (Fig. 2). The 3D seismic data thus permits a rare opportunity to analyse the distribution of extrusive bodies within a large mud volcano province. In addition to the analysis of the spatial and temporal distribution, the peculiar characteristics of the mud volcanism in this area combined with exceptional seismic imaging meant that a volumetric analysis could also be conducted on the plumbing system for individual mud volcanoes. The plumbing system in this context refers to the physical and process linkages between the source region for the remobilised fluids and solids, the conduit and the surface edifice. In particular, the seismic data allows the clear identification of the source region for the extruded mud through the recognition of geometrical characteristics that point to a specific location for the depletion zone for each mud volcano.

The depletion zone is defined here as the region where pronounced remobilisation of sediments has occurred within the source interval and where the remobilisation has allowed material to be depleted and transported out of that source interval. Stewart and Davies (2006) were the first to suggest that 3D seismic data could be deployed to pinpoint the depletion zone and to analyse the balance between the volume of the depletion zone and the extruded volume measured for a surface edifice. However, poor imaging at depth meant that they were not able to conduct such an analysis with the data at their disposal. We follow their suggestion, and attempt such a volumetric balance in an attempt to show the potential that 3D seismic data offers for the interpretation and analysis of mud volcano plumbing systems.

The paper sets out a basic description of the mud volcanoes and dimensions in relation to the main tectono-stratigraphic features of the host basin. In particular, the relationship of the mud volcanism to the thick succession of Messinian evaporites is emphasised. Previous studies have drawn attention to the impact of the Messinian Salinity Crisis (MSC) on basin hydrodynamics and sediment remobilisation phenomena in the Eastern Mediterranean (see Bertoni and Cartwright, 2015, for review), and we explore similar themes relating to the MSC in the Discussion. Most significantly from a perspective of hydrocarbon exploration, our analysis of the stratigraphic and spatial positions of over 380 mud volcanoes in this area shows a clear association between mud volcanoes emplaced during the Pliocene to Recent (post-MSC) with features developed at the base of the Messinian evaporites (Fig. 1). This implies that the formation of this huge number of mud volcanoes involved the development of conduits that bypassed the thick salt deposits. Since thick evaporite bodies are universally considered to be highly effective seals for petroleum accumulations (Downey, 1984), such an inference of vigorous and highly focused fluid flow through the evaporites raises interesting and broader resource questions linked to seal integrity.

We conclude the discussion with a more speculative discussion of the processes involved in mud volcano plumbing systems with particular emphasis on the mechanism of depletion of the source region. We assess the pressure regime required to drive mud volcanism and ask the question: what mechanisms pre-conditioned this region for mud volcanism and what impact did the Messinian Salinity Crisis (MSC) have on the basinal hydrodynamics?

2 Geological setting

2.1 Geological history and tectonic setting of the Nile Delta and NDSF

The study area is located on the western margin of the NDSF, a major sedimentary cone that built out over the passive continental margin of north-eastern Africa (Fig. 1). The formation of this passive margin followed earlier prolonged rifting in the Tethyan realm from the Triassic to the Early Cretaceous (Dolson et al., 2005). Convergence of the African and Eurasian plates in the Late Cretaceous led to the closure of the Tethys Ocean and compressional deformation that continued into the Early Cenozoic (Barber, 1981). The deep basement faults underlying this margin may have been partially reactivated during the Miocene rifting of the Suez-Red Sea Rift System (Loncke et al., 2006; Mascle et al., 2000; Loncke et al., 2004), and even later in the Neogene (Aal et al., 2000).

Propagation of the proto Nile Delta occurred as early as the late Eocene within the Western Desert, located to the west of the modern day Nile Delta and probably shed clastic sediments into the study through the Oligocene and into the Miocene (Said, 1962; Salem, 1976; Barber, 1981). The onset of the MSC at 5.9 Ma led to the deposition of > 1.5 km of evaporites over much of the deeper part of the Eastern Mediterranean (Druckman et al., 1995; Barber, 1981; Bertoni and Cartwright, 2006) (Fig. 3). Restoration of normal marine conditions across the Mediterranean Basin in the Pliocene (5.33 Ma) brought an end to evaporite deposition in the region (Hsü et al., 1977; McKenzie, 1999; Bertoni and Cartwright, 2007) (Fig. 3). The modern NDSF began to prograde in the Early Pliocene, and continued to build a large slope apron throughout the Pliocene to Recent, forming a large sedimentary wedge that covers c. 100,000 km^2 and extends northwards towards the Mediterranean ridge and Eratosthenes Seamount (Ross and Uchupi, 1977; Ryan and Cita, 1978; Salem, 1976).

The western NDSF, is characterised by a combination of active thin and thick skinned crustal tectonics (McKenzie, 1970; Sage and Letouzey, 1990; Mascle et al., 2000; McClusky et al., 2000). There are two structural regimes within this region: (1) regional basement tectonics associated with the Rosetta Fault system that is linked to lithospheric rifting (Aal et al., 2000) and; (2) gravity driven tectonics linked to downslope spreading of the Messinian evaporites. Two major basement fault trends are found beneath the NDSF, the Temsah trend (striking NW-SE) and the Rosetta trend (striking NE-SW and ENE-WSW) (Loncke et al., 2004; Aal et al., 2000). Both the thin and thick-skinned regimes have influenced the morphology of the continental slope (Gaullier et al., 2000; Loncke et al., 2006; Cartwright and Jackson, 2008).

2.2 Seismic stratigraphy of the western NDSF region

In the absence of direct well-calibration, it is only possible to describe the seismic expression of the various stratigraphic units within the study area, and draw some inferences from long range correlations to wells in neighbouring areas (Fig. 3). The stratigraphy is divided into three informal seismic-stratigraphic units, the pre-salt (all the seismically imaged stratigraphy beneath Horizon N, the regionally correlatable base of the Messinian Evaporites), the evaporite sequence itself, and the entire post-evaporite succession (Fig. 1B and Fig. 3). To aid description of the depletion zones, the pre-salt package has been divided into two sub-units.

2.2.1 Pre-Salt Unit, Sub-Unit PS1

This succession comprises reflections of variable amplitude and continuity (Fig. 1B). The presence of numerous seismic artefacts (amplitude attenuation and scattering, migration smiles and distortion due to overlying velocity anomalies) leads to much poorer quality imaging relative to shallower intervals. Large basement faults transect through Sub-Unit PS1, resulting in a horst

and graben structure possibly associated with the successive episodes of rifting during the Triassic (Morelli, 1978; Hirsch et al., 1995; Dupre et al., 2007) (Fig. 1B).

2.2.2 Pre-salt Unit, Sub-Unit PS2

This unit has a wedge-shaped geometry with an increasing thickness towards the northeast (Fig. 1B) and is characterised by a slope-healing, onlap wedge configuration (sensu Prather et al. (1998). The basal bounding reflection of Sub-Unit PS2 is a regionally continuous positive, high amplitude reflection of unknown age, marked by basal onlap (Fig. 1B). Sub-Unit PS2 is bounded upwards by Horizon N, a regionally continuous, high amplitude and negative reflection that marks the base of the Messinian across much of the Mediterranean region (Bertoni and Cartwright, 2005; Bertoni and Cartwright, 2006; Bertoni and Cartwright, 2007; Duggen et al., 2003) (Fig. 1B and Fig. 3). Sub-Unit PS2 is marked by seismic facies that are typically variable amplitude but with high lateral continuity, allowing local correlations to be made with ease (Fig. 1B). The coherence, continuity and amplitude of these reflections decreases towards the top of the succession (Fig. 1B). The sediments at the top of Sub-Unit PS2 immediately beneath the evaporite succession are at youngest Tortonian in age (Fig. 3). Extrapolation from other well calibrated pre-Messinian successions in the Levant Basin suggests that the uppermost section of Sub-Unit PS2 most likely consists of a marly or clay rich interval (Bertoni and Cartwright, 2005; Grasso et al., 1982) (Fig. 3). Several of the deep crustal faults that transect Sub-Unit PS1 also cut across Sub-Unit PS2 and propagate upwards to Horizon N (Fig. 1B).

2.2.3 Messinian Evaporite Sequence

This thick stratigraphic interval is part of the regionally extensive Messinian Evaporite Sequence that can be traced across the Mediterranean (Fig. 3). In the study area it is wedge

shaped, increasing in thickness and gently dipping towards the North (Bertoni and Cartwright, 2005; Grasso et al., 1982; Barber, 1981) (Fig. 1B). The interval locally exhibits an average interval velocity of c. 4500 m/s, contains discontinuous high amplitude reflections but is primarily composed of a transparent, discontinuous and chaotic seismic facies, typical of the halite rich Messinian succession documented further to the East (c.f. Bertoni and Cartwright (2007) (Fig. 1B and Fig. 1C).

The top of the evaporite succession is characterised by a high amplitude reflection known as Horizon M that is regionally correlatable (Bertoni and Cartwright, 2007; Loncke et al., 2004) (Fig. 1B and Fig. 3). Horizon N and Horizon M demarcate the onset of the MSC and climax of the MSC respectively (Fig. 1B and Fig. 3). These two reflections are both highly irregular in geometry on a kilometre scale with numerous depressions developed at frequent intervals (Fig. 1B and Fig. 4).

2.2.4 Post-Salt Unit

This seismic-stratigraphic unit comprises sediments that are deposited within the more distal and aggradational region of the NDSF and are Pliocene to Recent in age. The seafloor dips in a NW direction and the unit exhibits a gradual increase in thickness distally Fig. 1B. It is predominantly composed of coherent, laterally continuous reflections whose seismic facies is typical of the widely developed hemipelagites seen further to the East in the main gas producing areas of the Nile Slope (Dolson et al., 2005; Samuel et al., 2003) (Fig. 1B).

The unit is bound at its base by Horizon M and at its top by the seafloor (Fig. 1B and Fig. 3). The seafloor within this study area is generally smooth but is disrupted by numerous pockmarks, and by the extrusion of 110 mud volcanoes, some of which may currently be active judging from the imaging of sediment flows on their flanks and absence of onlap onto their upper surfaces (Fig.

2 and Fig. 5B). A channel/levee complex is developed in the NE of the study area, and a series of thin skinned growth faults are found in the SW (Fig. 2). A further 276 mud volcanoes are buried at various depths throughout the post-salt succession, particularly in the region of the Menes Caldera (see Fig. 2 and Fig. 4). This prominent seafloor depression measures 8 km in diameter has been previously documented as a highly active area for mud volcanism (Mascle et al., 2014; Pierre et al., 2014; Dupré et al., 2014; Giresse et al., 2010; Huguen et al., 2009) (Fig. 2 and Fig. 4).

3 Data and methodology

The high resolution 3D seismic volume used for this study consists of time and depth migrated data that covers an area of ~4300 km^2 in water depths ranging from c. 2500-3000 m. The binset dimensions of 12.5 x 6.25 m yield a lateral resolution of c. 25 m throughout the post-salt succession. The data is zero phased with SEG normal polarity, i.e. an increase in acoustic impedance is represented by a positive amplitude response. Vertical seismic resolution is ~3 m (Frequency – 125 Hz; Velocity – 1520 m/s) at the seabed, ~8 m (Frequency – 60 Hz; Velocity – 1800 m/s) within the post-salt succession and ~30 m (Frequency – 35 Hz; Velocity – 4400 m/s) at the Top Messinian. P-wave velocity values are derived from pre-stack depth migrated velocity data (Fig. 1C).

The data was interpreted using Schlumberger's GeoFrame and Petrel software. All the significant, laterally correlatable horizons were tracked throughout the survey area, and horizon maps were computed in two way travel time (TWT) and in depth. A standard suite of attributes (RMS Amplitude, Coherence, Dip, see Brown et al. (2004)) were computed and displayed for each mapped horizon, and used to constrain the interpretation of geological features such as mud volcanoes, faults and pockmarks.

Dimensional parameters (diameter, height and volume) were recorded for the 386 mud volcanoes interpreted within this survey area. The general shape of these mud volcanoes is approximately conical in the vast majority of cases and their volumes were calculated from their basal radius using the equation for the volume of a cone (Fig. 5). Many of the buried mud volcanoes have been deformed from their original shapes by subsidence during or after extrusion (e.g. Fig. 4). These now have lensoid or inverted conical shapes, and in these cases the volumes were calculated by taking the maximum vertical thickness of the lensoid body or inverted cone, and flattening the basal reflection using the interpretation software such that a conical volume could be computed.

Other volumetric parameters recorded here include the volume within depressions at the top of Sub-Unit PS2. These values were acquired by first calculating the volume between the gridded surfaces of the base of Sub-Unit PS2 and Horizon N, and second calculating the volume between the base of Sub-Unit PS2 and an interpolated surface that forms the best fit to the relief of the region immediately surrounding the depression (Fig. 6). The first volume value is then subtracted from the second, giving a final calculated volume of the depression (Fig. 6). This technique has been used previously to compute the shapes of depressions associated with evaporite dissolution in the Levant Basin (Bertoni and Cartwright, 2005).

4 Results

4.1 Seismic expression, dimensions and geometry of mud volcanoes

Mud volcanoes are readily interpretable within the 3D seismic volume as distinct bodies with lensoid (when buried), inverted conical or conical geometry. They are easily identifiable using layer parallel or horizontal attribute slices, or indeed, from RMS amplitude or coherence attribute images because of their circular to elliptical planform (Fig. 4 and Fig. 5). In cross-section, they are invariably thickest in their centre and thin towards their flanks where upper and basal bounding reflections merge into a single reflection (Fig. 5). Their seismic expression is thus similar to many other previously described mud volcanoes (Dimitrov, 2002; Fowler et al., 2000). Onlap onto the upper bounding reflection is commonly observed, except where deeper burial and distortion due to subsidence and compaction renders this uninterpretable. This observation confirms that an edifice was built at the seabed and subsequently onlapped, implying that they are indeed the product of surface extrusion. Reconstruction of this surface relief suggests a range of slope angles from 5° – 30° (Fig. 4 and Fig. 5). In contrast, many of the examples occurring nearer to the seabed or at the modern seabed exhibit basal surface slopes that dip inwards at angles ranging from 1° - 30°, resulting in a centrally depressed and bowl shaped base (Fig. 5). It is notable that in many cases, the substrate underlying the mud volcanoes is also deformed into a concordant bowl shape, where the geometry of the depressed reflections mimics that of the basal surface of the mud volcanoes (Fig. 4 and Fig. 5)

The internal seismic facies of the mud volcanoes is generally chaotic and discontinuous, low frequency and low amplitude (Fig. 5), similar to that of other mud volcanoes from the Central Mediterranean Ridge and NDSF which have been described as “acoustically transparent” (Huguen et al., 2004; Giresse et al., 2010). Occasionally, continuous stratification and high amplitude

anomalies can be observed within the mud volcanoes. In contrast, the upper and lower bounding reflections are typically continuous and high amplitude (Fig. 5) .The lateral margins of the mud volcanoes are typically sharply defined at the convergence of the upper and lower bounding reflections with no evidence of interdigitation with the reflections of the host succession (Fig. 5).

A total of 386 mud volcanoes have been mapped within the study area at various stratigraphic levels within the post-salt succession and at the present day seabed (Fig. 2 and Fig. 4). Their diameter ranges from c. 550 m to c. 5660 m, and their height (from their basal reflection to upper reflection, (Fig. 5)) ranges from c. 25m to c. 510 m. A plot of diameter vs height demonstrates that some mud volcanoes display a large diameter but low relief, while very few mud volcanoes exhibit small diameter but significant topography (Fig. 7). Although the data points display a scatter that increases with diameter, there is a slight correlation between mud volcano diameter and height (Fig. 7).

4.2 Spatial and temporal distribution of mud volcanoes

The study area is delimited by the lateral extent of the seismic survey so it is not clear what the full lateral extent of this mud volcano province might be. Even in this relatively small area, the 386 mapped cones gives a density of c. 9 mud volcanoes/100 km^2, which is relatively high when compared to other large mud volcano provinces such as onshore Azerbaijan or offshore Barbados where there are as many as 450 mud volcanoes/150,000 km^2 (c. < 1/100 km^2) (Milkov, 2000; Brown and Westbrook, 1988; Yakubov et al., 1971). Of these mapped cones, about a third were emplaced in the Holocene, and the remainder occur throughout the Pliocene-Pleistocene succession.

The areal distribution of the 386 mud volcanoes presented in Fig. 2 shows that the majority of the mud volcanoes are concentrated within the central region of the study area where they are densely packed (average density = c. 15 mud volcanoes/100 km^2), and occasionally show alignments in distribution. The marginal areas of the survey do contain some mud volcanoes, but at a greatly reduced density (average density = c. 1 mud volcano/100 km^2). There is no obvious correlation between the seismically imaged geology and this density distribution e.g. no correlation with isopach values or reflection configurations of the Messinian Evaporite or Pre-Salt Units. It is interesting to note that the reduced density in the south-western corner of the survey area coincides with a region of marked growth faulting in the Post-Salt Unit, detaching into the salt (Fig. 1B and Fig. 2)

To further examine the distribution of mud volcanoes their spatial packing is analysed within a sub region of the study area referred to here as sub region 1 (SR1) that contains 44 mud volcanoes within an area of c. 284 km^2 (Fig. 8B). Within SR1 multiple mud volcanoes can be observed emplaced along the same seismic reflection at numerous stratigraphic levels (Fig. 8A and Fig. 8C). Based on average sedimentation rates of 200 m/Ma and a seismic resolution of 10 m it can be estimated that in order to form a single reflection of ~40 m it would take 200 kyrs, which implies that mud volcanoes emplaced along a single seismic reflection will have formed at a maximum of 200 kyrs apart. Nearest neighbour distances between mud volcanoes along single mapped horizons within SR1 range from c. 2 km in Horizon 1 (H1) and Horizon 2 (H2) to 9 km in Horizon 4 (H4), and frequently < 1 km when analysing all mud volcanoes at all stratigraphic levels (Fig. 8B and Fig. 8C). These relatively small nearest neighbour distances imply that these mud volcanoes have formed in close spatial relation to one another, resulting in their dense packing. Due to their close packing distance it is relatively common for the flanks of mud volcanoes to

spatially overlap, however despite their close spatial relationship it is unusual for more than one mud volcano to be observed stacked with their centres vertically aligned (Fig. 8).

4.3 Deformation and depletion associated with mud volcanoes

One of the most striking features of the base of the Messinian Evaporites is the highly irregular geometry exhibited by Horizon N. The highly irregular surface seen in cross section (e.g. Fig. 4 and Fig. 9) has two characteristic patterns in planform, (1) sub-circular depressions with typical relief of 200-300m but occasionally > 500m, and (2) more elongate irregular, serrate pattern with a clearly erosional relief of 200-700 m (Fig. 9 and Fig. 10A). These erosional features are recognised from the obvious and angular erosional truncation of reflections within Sub-Unit PS2 by Horizon N (Fig. 9A and Fig. 9B). In planform, many of these erosional features have a prominent N-S strike (Fig. 10A), parallel to the dominant slope direction immediately prior to the Messinian (Barber, 1981). These relationships are indicative of erosion under surface conditions, and we interpret them to have resulted during the initial drawdown of the Mediterranean at the beginning of the MSC (c.f. Barber (1981)). Importantly there is no spatial association between mud volcanoes and these erosional base-salt depressions, and additionally, above these depressions, Horizon M is discordant to Horizon N and there is an increase in the thickness of the evaporite succession (Fig. 9A).

Circular to sub-circular base-salt depressions exhibit contrasting stratal geometries to those interpreted as being linked to erosion during early drawdown. They occur mainly within the central region of the study area, similar to the distribution of mud volcanoes, and there is a striking correspondence in the details of their distribution (Fig. 9C and Fig. 10A). Furthermore, Horizon M is relatively concordant with Horizon N over these base-salt depressions, as are some of

the more continuous intra salt reflections within the evaporite succession (Fig. 9C), suggesting that the timing of the formation of the depression post-dates the MSC.

The stratal geometry at Horizon N is frequently ambiguous along the margins of the depressions. Reflections within the immediate pre-salt of Sub-Unit PS2 can be seen to clearly exhibit a change in dip towards the depression and display greater concordance with Horizon N when compared with the erosional features at Horizon N that are noted above. Unfortunately multiple reflections and imaging problems at the base of the salt (in both the time and depth migrated volumes) mean that this relationship is not always sharply defined (Fig. 9C and Fig. 9D). Significantly, there is commonly localised decrease in the thickness of the low amplitude Sub-Unit PS2 directly beneath the depressions (Fig. 9C). These stratal relationships are inconsistent with an interpretation of their formation by erosion.

Superficially at least, these circular to sub-circular depressions at Horizon N bare resemblance to the giant pockmarks that formed during the initial drawdown by gas escape and that have been identified further to the East in the Levant Basin (Bertoni et al. 2013). However, the depressions interpreted as pockmarks by Bertoni et al. (2013) were infilled by Messinian Evaporites, whereas the vast majority of the circular depressions in the study area have a depression at Horizon M that matches that at Horizon N. An origin for these circular to sub-circular depressions as pockmarks can therefore be discounted.

As an alternative to either surface erosion or pockmark formation, it is interpreted here that the planform and cross-sectional geometry and stratal relationships at Horizon N are consistent with the description of ‘depletion zones’ associated with mud volcanoes previously interpreted in other mud volcano provinces (Stewart and Davies, 2006; Istadi et al., 2009; Fukushima et al., 2009). These ‘depletion zones’ have only rarely been identified and linked to a

specific source region for the extruded mud, the criterion being that the mud volcano is underlain by reflections with a concave upwards geometry formed due to a bowl-shaped region of local subsidence directly overlying a stratigraphic layer that clearly displays thinning as a result of volume loss at depth (Stewart and Davies, 2006; Istadi et al., 2009; Fukushima et al., 2009) (Fig. 11). A 'depletion zone' is referred to here as the region (volume) of a source stratigraphic layer from which a volume of sediment has been remobilised and extracted during the extrusion of the mud slurry that is transported out of that layer to form the mud volcano.

By carefully comparing the time and depth maps of Horizon N with the mapped positions of all the mud volcanoes, it is found that 338 of the 386 mud volcanoes in the study area overlie a base-salt depression with stratal geometries that are indicative of depletion zones (Fig. 10A and Fig. 11A). This strong spatial correlation implies that the zone from which sediment has been withdrawn and depleted during mud volcanism is primarily extracted directly beneath the mud volcanoes within the pre-salt succession and not from a broader region perhaps several times wider than the edifice dimensions. Of the 338 mud volcanoes that overly a base-salt depression, 327 also overlie a top-salt depression (Fig. 10B and Fig. 12). Depletion of a source layer directly beneath a mud volcano would be expected to lead to subsidence of the entire overburden above the depletion zone, albeit with likely diminishing impact at shallower levels (Fig. 6 and Fig. 11), so this spatial correlation between top and base salt depressions and mud volcanoes (e.g. Fig. 12) adds additional support to the interpretation here of depletion zones within Sub-Unit PS2.

4.4 Volumetric analysis

The volume of individual mud volcanoes ranges from c. 0.1 km^3 to c. 3.3 km^3, but it should be noted that errors in these values are probably of the order of 20% mainly due to the lack of any

attempt to decompact the buried edifices. It was not considered worthwhile to decompact the volumes given the complete absence of any lithological calibration. Minor errors of up to 5% are estimated for accuracy of picking of upper and lower bounding surfaces and volume computations. The total volume of extruded mud from all 386 mud volcanoes amounts to c. 210 km^3. The median and average volumes for single volcanoes are c. 0.4 km^3 and 0.5 km^3 respectively.

A representative example of a single edifice that can be unambiguously connected to an underlying depletion zone is that of Mud Volcano 197 (Fig. 13). This single mud volcano exhibits concave upwards reflections within the post-salt succession, and at Horizon M and Horizon N, together with anomalous thinning within Sub-Unit PS2 directly beneath (Fig. 9C and Fig. 13). The depletion zone is identified as an area of anomalous thinning within Sub-Unit PS2 that is spatially correlatable with a base-salt depression and overlying downsagging reflections of Horizon M and the post-salt succession beneath a mud volcano (Fig. 13). The first clear and continuous reflection within Unit PS2 that does not display sagging geometry generally resides within towards the base of the succession and represents the base of the depletion zone (Fig. 13). Imaging issues associated with seismic artefacts such as velocity 'pull up' or 'push down', scattering and attenuation, low signal to noise ratios and reflected refractions within the pre-salt succession of Sub-Unit PS2 can make identifying the base of the depletion zone challenging. The margins of the area of anomalous thinning within the immediate pre-salt succession are interpreted here to define the margins of the depletion zone (Fig. 13), which in the case of mud volcano 197 has formed a circular to sub-circular depletion zone (Fig. 13).

In areas where multiple mud volcanoes have formed within close proximity to one another, an amalgamation of circular to sub-circular depletion zones results in more irregularly shaped base-salt and top-salt depressions and complimentary areas of anomalous thinning within Sub-

Unit PS2 (e.g. see Fig. 12, SR2). This amalgamation of depletion zones results in geometries that are far more complex than in the single case of Mud Volcano 197 shown above, and could help explain the challenge of identifying depletion zones more generally, and explain why so few have been described previously. Other reasons may be attributed to the fact that mud volcano systems are comprised of numerous components, such as the depletion zone, the interpretation of which is intrinsically linked to seismic imaging quality and areas of acoustically turbulence that often shroud the region underlying mud volcanoes and their conduits (Stewart and Davies, 2006; Dimitrov, 2002). An additional consideration is that mud volcanoes are long lived mud extrusions that have the potential to last for several thousands to millions of years, progressively extruding an increasing volume of mud slurry with time (Calves et al., 2010). The stage of eruption and subsequently volume of mud withdrawn from a source region will therefore vary depending on the stage of a mud volcanoes eruptive life. Hence identifying the depletion zone of a mud volcano may prove challenging during the earlier stages of its prolonged evolution or if the overall scale of the mud volcano is relatively small.

It has previously been suggested that it should be possible to volumetrically balance a depletion zone and the extruded material within a mud volcano (Stewart and Davies, 2006). Given that the stratal geometries at Horizon N point to the likely depletion region being within Sub-Unit PS2, it is then straightforward to compute the volume that has been depleted from this interval using a simple subtraction of the appropriate map grids. The procedure requires that depletion zones are identified and delineated as 'geobodies' from the stratal geometry within Sub-Unit PS2. The volume of sediment withdrawn from the succession can be attained by firstly calculating the volume between the base of Sub-Unit PS2 and a smoothed and interpolated Horizon N, where the interpolation restores the stratigraphic relationships prior to depletion (Fig. 6). The actual volume

between the base of Sub-Unit PS2 and Horizon N is then calculated. Finally, the difference between the hypothetical volume and actual volume provides an estimate for the volume of sediment withdrawn within a depletion zone.

To illustrate the approach outlined above, the resulting volume balance was computed for two sub regions within the study area named sub region 1 (SR3) and sub region 2 (SR4), each of which cover an area of c. 180 km^2 and contain 33 and 64 mud volcanoes respectively (Fig. 10A). These areas were selected for the quality of the imaging in the pre-salt. The combined extruded volume (Ve) of the mud volcanoes within SR3 and SR4 is c. 26.4 km^3 and 25.1 km^3 respectively, and the volume of the depletion zones (Vd) within SR3 and SR4 are 22.6 km^3 and 21.1km^3 respectively. The extruded and depleted volumes thus match remarkably closely, which is even more notable given the likely errors. We estimate the error in these values is of the order of 20% to reflect the velocity artefacts associated with pre-salt horizon picking and volume loss due to dewatering during the compaction of extruded edifices during burial. The closeness of this volumetric balance also lends credence to the interpretation of these depletion zones and demonstrates the potential for this approach in other mud volcano plumbing systems.

5 Discussion

Evidence presented here from the mapping of 386 individual edifices within the western slope of the Nile Cone demonstrates the prolificacy of this mud volcano province. The analysis conducted raises a number of fundamental questions regarding the source of the mud, pore fluid and possibly gas that constitute the extruded slurry, and the scale and stratigraphic extent of the remobilised source region supplying this province, and individual edifices. Perhaps more

fundamentally, the evidence presented on the geometry of the depletion zones raises questions relating to the process of remobilisation and transport of the slurry from the depletion zone to the conduit. From the perspective of extruded volumes, the number of mud volcanoes province is comparable to some of the largest mud volcano provinces in the world (Kopf, 2002; Jakubov et al., 1971; Brown and Westbrook, 1988; Bagirov et al., 1996), so insights gained here may be relevant in these other provinces, where it has not been possible to undertake 3D volumetric balancing.

5.1 Sources and remobilisation of mud

Direct evidence of the origin of solid components, fluid and gas within the extruded mud slurry has been obtained from different sampling methods at the seabed on the modern mud volcanoes. Piston core samples from mud volcanoes at the seafloor within this study area are reported to contain rock clasts that are up to Cretaceous in age and directly imply a pre-salt origin (Dupré et al., 2014; Mascle et al., 2014; Giresse et al., 2010). Hot saline brine pools associated with these mud volcanoes have been interpreted to have formed due to dissolution of the Messinian evaporites by ascending fluids of pre-salt origin (Mascle et al., 2014; Huguen et al., 2009; Dupré et al., 2014; Giresse et al., 2010). Geochemical analysis of gas seepage samples have been found to be mainly thermogenic in origin and of varying maturity, some of which are of very high maturity and considered to be indicative of a deep pre-salt source (Prinzhofer and Deville, 2011; Pierre et al., 2014).

The seismic data provides indirect evidence supporting these more direct surface sampling methods for the source of the greater part of the slurry volume to have come from below the Messinian Evaporites. There is no evidence of depletion at any scale within the Post-Salt Unit, or the Messinian Evaporites themselves. Furthermore, there are many edifices that occur almost

directly on Horizon M, i.e. they were extruded immediately after the MSC, and these can only have sourced from the Pre-Salt Unit. There is no evidence that any significant clastic bodies were interbedded within the Messinian Evaporites, since all the intra-salt reflections are only of very local extent and velocity analyses of these reflections shows a high interval velocity, typical of evaporites (Fig. 1C).

Although not calibrated by wells, we suggest that the interpretation of stratal geometries that are consistent with depletion zone geometries observed previously is the strongest evidence for the stratigraphic location of the source region (Fig. 9C, Fig. 11 and Fig. 13). It is therefore proposed that Sub-Unit PS2 is the main source of the remobilised mud for the mud volcanoes. The close match between depletion volume (Vd), and extruded volume (Ve), provides quantitative support for this argument (Fig. 6). Sub-Unit PS2 is most likely Miocene in age, but we cannot exclude older units within the Cenozoic being present in this source interval. Based on a qualitative analysis of deep structure and mud volcano distribution further East in the Nile Cone, Bentham et al. (2006) proposed that the main source region is the Tortonian deep-water deposits, which are regionally mud prone. Even further east, in the Levant Basin, Frey Martinez et al (2007) reported large scale remobilisation of Oligo-Miocene canyon fill deposits to form muddy intrusions. It is evident therefore that this mid Cenozoic interval resulted in mud-dominated deposition in the SE Mediterranean, and that the characteristics of the deposition resulted in the potential for later remobilisation. However, it is plausible that fluids and clasts derived from potentially multiple other intervals within the pre-salt succession could have contributed to the gross extruded volume, as suggested by the presence of clasts up to Cretaceous in age (Mazzini et al., 2009; Mazzini et al., 2007; Tanikawa et al., 2010; Mazzini et al., 2012; Giresse et al., 2010).

5.2 Overpressure generative mechanisms

The formation of mud volcanoes has been fundamentally linked to the generation of an overpressured source region (Kopf, 2002). Pressure prediction within this study area is unfortunately not possible in absence of well and stratigraphic information. However, velocity data reveals low p-wave velocity of < 2000 m/s at burial depths of 3-4 km within the pre-salt, which is not only significantly lower than the overlying evaporites but also the post-salt succession (Fig. 1). A velocity inversion such as this could be indicative of significant undercompaction and overpressure (Calves et al., 2010; Magara, 1978). Present day hard overpressure within pre-Messinian sediments has been invoked to be widespread across many parts of the Eastern Mediterranean (Dolson et al., 2001; Loncke et al., 2004; Mascle et al., 2014). So what mechanisms could potentially have led to overpressuring of the source interval (Sub-Unit PS2) in the study area on the appropriate time scale?

Disequilibrium compaction has been widely documented elsewhere as a vital mechanism for generating the requisite overpressure in the source region (Milkov, 2000; Osborne and Swarbrick, 1997). This mechanism is certainly viable for overpressure generation in the pre-salt in general within this study area, with recent estimates placing the deposition of the > 1.5 km thick Messinian Evaporite at between 300 and 600 kyrs at extremely high sedimentation rates of c. > 4 cm/yr (Hsü et al., 1977; McKenzie, 1999; Bertoni and Cartwright, 2007; Duggen et al., 2003; CIESM, 2008). When combined with the inherently low permeability of the evaporites, undercompaction and significant elevation of pore fluid pressure would be almost inevitable (Kopf and Behrmann, 2000; Osborne and Swarbrick, 1997). The lateral extent of the evaporite seal to the underlying units would most likely have impeded the escape of overpressured fluids thus provided the

priming mechanism for significant and laterally extensive overpressure conditions within Sub-Unit PS2 and potentially the deeper successions too.

It is also conceivable that hydrocarbon generation may have played a role in overpressure generation. The lack of calibration means that the organic carbon content of Sub-Unit PS2 is unknown, but pre-salt source rocks are well known from the region, and fuel a major pre-salt petroleum play some 100 km to the East of the study area (Vandré et al., 2007). Importantly, methane-rich and oily hydrocarbon-rich hot brine and mud samples taken from several mud volcanoes within this study area provide irrefutable evidence for the inclusion of hydrocarbons within the ascending mud slurry (Pierre et al., 2014; Dupré et al., 2014; Huguen et al., 2009). The generation and migration of hydrocarbons could potentially lead to entrapment beneath the sealing evaporites and accumulation within the upper section of Sub-Unit PS2, providing there were reservoirs at this level. This could have resulted in a build-up in pore fluid pressure that has contributed to the generation of overpressure required for mud volcanism. Such a mechanism might be more localised, than disequilibrium compaction, and would favour overpressure development in reservoirs rather than in the encasing mud-prone sediments themselves. On balance therefore, we favour disequilibrium compaction resulting from the MSC as the most likely overpressuring mechanism priming the mud volcanism, possibly with augmentation from more local hydrocarbon buoyancy.

5.3 The processes of remobilisation

The extrusion of sediments as a slurry implies that sediments at depth have been remobilised (Kopf, 2002). What, if anything can we infer about the processes required to

remobilise large volumes (often > 1 km^3 of deeply buried and compacted sediments) and transport them 1000 m or more through a low permeability evaporite succession?

Fluidisation has previously been proposed as a process associated with the formation of mud volcanoes (Nermoen et al., 2010; Lorenz, 1975; Brown, 1990). Sediment can be mobilised via fluidisation where drag is exerted on the sediment of a host succession by migrating pore fluids that are of a sufficient velocity to exceed the settling velocity of the granular material, and subsequently entrap grains in the migrating flow (Cartwright and Santamarina, 2015; Lowe, 1975; Judd and Hovland, 2007). However, it is difficult to imagine how the necessary flow velocity for fluidization can develop within a layered sedimentary succession where the intrinsically low permeability restricts fluid flow (Cartwright and Santamarina, 2015).

Liquefaction presents an alternative mechanism for mobilisation with the potential to mobilise large volumes of sediment from deeply buried stratigraphic layers (Lawrence and Cartwright, 2010; Tanikawa et al., 2010). Liquefaction arises when there is a loss of friction between grain particles in a loosely packed framework and the grains become temporarily supported by the fluid (Lowe, 1975; Brown, 1990). In order for liquefaction to occur, the effective stress must equal zero and the fluid pressure must therefore equal the maximum compressive stress acting on the sediment (Judd and Hovland, 2007; Brown, 1990). Hence pore fluid pressure must equal or exceed the overburden stress for liquefaction to occur (Judd and Hovland, 2007; Tanikawa et al., 2010).

Liquefaction is most common in shallow sand rich sequences where it is easier for fluid pressure to reach lithostatic pressure for example during seismic shaking during earthquakes (Tanikawa et al., 2010), but has not been demonstrated for more deeply buried muddy sedimentary layers. Liquefaction within deep layers is thought to be related more to the

generation of overpressure in layers of low permeability (Kopf, 2002; Tanikawa et al., 2010). Dynamic fluctuations in pore fluid pressure sufficient to liquefy part of a source region could conceivably be caused by a range of mechanisms including earthquakes (Tanikawa et al. 2010), rapid loading or unloading by eustatic changes (Hermanrud et al., 2013) or by sudden depositional events of substantial sediment thickness (e.g. mass transport deposits) (Lawrence and Cartwright, 2010; Riis et al., 2005). The presence of even modest amounts of methane in solution in the pore fluid could have had profound consequences and aid the process of dynamic liquefaction in the source unit**s** (c.f.Imbert et al. (2014)). These essentially rapid overpressuring mechanisms may have had a role in taking the source region to the necessary state to achieve local liquefaction, but they would have been superimposed, in all likelihood, on a system that was already highly overpressured, possibly with a large, highly overpressured region developed within the entire pre-salt succession, such that only a minor trigger of a rapid event would be needed to exceed the necessary threshold.

5.4 Forming the depletion zone

One of the most important observations made in the results section is the geometry of the depletion zones and their stratigraphic position within the pre-salt (Fig. 13 and Fig. 14). This raises important questions about the process of forming a depletion zone, with wider implication for depletion and mud volcano formation in general.

The geometry of the depletion zones is governed by the region of the pre-salt succession where liquefaction has occurred. In all cases where seismic data quality permits a clear identification of a loss of material from Sub-Unit PS2, it has been shown that depletion would most likely have occurred concentrically in a zone directly beneath the mud volcano that it

supplied. Concentric feeding strongly suggests that whatever process occurs, it links directly into the conduit, and potentially propagates radially outwards from the conduit. This type of radial outward propagation is strongly reminiscent of drainage from an overpressured aquifer, as has been suggested for the origin of blow out pipes by Moss et al. (2012).

The consistently circular to sub-circular shape in planform and gradually sloping sides of the depletion zones, opposed to more irregularly shaped and abruptly sloped depletion zones such as the craters observed by Lawrence and Cartwright (2010) within the Møre Basin offshore Norway, argues against sudden liquefaction of the entire volume of the depletion zone. An alternative process is one of episodic outward propagation of the depletion zone via a dynamic liquefaction mechanism. This would be a cyclic process that involves a progressive increase in pore fluid pressure that leads to liquefaction and mobilisation of a small volume, the removal of which triggers the subsequent liquefaction of a further volume, and so on (Terzaghi et al., 1951) (Fig. 14). This type of multi-episode liquefaction would cause the liquefaction front and subsequently the depletion zone to grow out from a central starting point. A process such as this may explain the circular to sub-circular geometry in planform of depletion zones, as the liquefied slurry is mobilised towards the conduit (Fig. 14). The episodic processes associated with dynamic liquefaction may also influence the flux and episodicity of these mud volcanoes and contribute toward the internal stratification described within.

The reflections that comprise the post-salt succession and notably Horizon M display a bowl-shaped concave upwards geometry beneath extruded mud volcanoes and above the depletion zones (Fig. 5, Fig. 12 and Fig. 13). The geometry of these reflections suggests that the various stages of liquefaction and withdrawal of mud from depletion zones also coincides with subsidence and collapse of the overburden above Horizon N (Fig. 14). The subsidence and collapse of this

overburden also offers an elegant process to further disturb the underlying source region, resulting in a deformation induced liquefaction mechanism and subsequent overpressuring that could initiate the next stage of remobilisation and outward growth of the depletion zone (Fig. 14). Other mechanisms that could have contributed to the formation of depressions at Horizon M are the localised gravitational loads applied by the mud volcanoes and dissolution of the evaporites. Applying sufficient vertical pressure from the loading of mud volcanoes could cause horizontal salt flow or “salt expulsion” perpendicular to the pressure direction (Hudec and Jackson, 2007). Brine pools at the seafloor associated with mud volcanoes within this region indicate that the Messinian evaporites have been dissolved within the ascending fluids (Mascle et al., 2014; Huguen et al., 2009; Dupré et al., 2014; Giresse et al., 2010).

Finally, the recognition of a major mud volcano province that has been active over a prolonged period of > 5 million years where the mud has been sourced beneath a > 1.5 km thick layer of evaporites has major implications for how we view thick evaporites as potential seals in petroleum systems. The general belief that thick evaporite sequences represent almost impermeable barriers to upward fluid migration (Downey, 1984) does not seem to hold true here in the Eastern Mediterranean, given the frequent and catastrophic breaching of this thick succession of evaporites. Although, as argued here, the conditions for overpressure generation in the source interval may well have been exceptional, resulting as they did from the extreme loading and unloading of the region by drawdown, rapid evaporite deposition and reflooding, we see no reason why similar catastrophic seal breach of thick evaporites might not have occurred in other basins, and provide windows for deeply generated hydrocarbons to bypass the seal and charge shallower reservoirs. This may open up new possibilities for exploration in some basins containing thick salt successions.

6 Conclusion

A total of 386 mud volcanoes are distributed throughout the post-salt succession of a 3D seismic dataset from the western slope of the Nile Cone, Eastern Mediterranean. Due to the exceptional scale of mud volcanism within the El Dabaa study area, it is suggested here that this region should be considered as among the largest mud volcano provinces in the world. The main conclusions from the analysis conducted here are as follows:

- The primary source of mud for the mud volcanoes is believed to be from Sub-Unit PS2, which is the succession directly beneath the sealing Messinian evaporites.
- The basinal hydrodynamic effects of the MSC due to rapid deposition of low permeability evaporites is likely to have resulted in the generation of significant and long lasting overpressure within Sub-Unit PS2 directly beneath the Messinian evaporite succession.
- Hydrocarbon generation, earthquakes and various loading and unloading events pose the potential to cause fluctuations in pore fluid pressure within the already overpressured succession of Sub-Unit PS2 over the last ~5.3 Ma, resulting in numerous episodes of liquefaction, sediment remobilisation and ultimately mud volcanism.
- There is a strong spatial relationship between mud volcanoes and underlying depletion zones. 3D seismic data has facilitated the quantitative volumetric analysis of depletion zones for the first time in any analysis of mud volcanism.
- Depletion zones are suggested to have radially propagated, potentially via a dynamic liquefaction process that results in their final geometry.

- It is highly plausible that many more mud volcanoes exist at the seafloor and within the subsurface within the western province, beyond the margins of the survey region used in this study. There is, therefore, potential in the future to further expand the analysis and understanding of this mud volcano province.
- Seal breaching across the > 1000m thick evaporite sequence took place repeatedly in the past 5 million years, demonstrating that evaporites are not the perfect seals that they are often assumed to be.

Acknowledgments

We would like to thank Statoil for provision of the data used in this study and NERC for award number BW22003102 that supported this research. We are also grateful to Schlumberger for provision of the IESX and Petrel software suites for the seismic interpretation.

References

AAL, A. A., EL BARKOOKY, A., GERRITS, M., MEYER, H., SCHWANDER, M. & ZAKI, H. 2000. Tectonic evolution of the Eastern Mediterranean Basin and its significance for hydrocarbon prospectivity in the ultradeepwater of the Nile Delta. *The Leading Edge,* 19**,** 1086-1102.

BAGIROV, E., NADIROV, R. & LERCHE, I. 1996. Flaming eruptions and ejections from mud volcanoes in Azerbaijan: Statistical risk assessment from the historical records. *Energy exploration & exploitation,* 14**,** 535-583.

BARBER, P. M. 1981. Messinian subaerial erosion of the proto-Nile Delta. *Marine Geology,* 44**,** 253-272.

BENTHAM, P., PASLEY, M. & BIRT, C. The style and timing of mud volcanism in the offshore Nile Delta, Egypt. Paris 2005 AAPG International Conference and Exhibition, 2006.

BERTONI, C. & CARTWRIGHT, J. 2005. 3D seismic analysis of circular evaporite dissolution structures, Eastern Mediterranean. *Journal of the Geological Society,* 162**,** 909-926.

BERTONI, C. & CARTWRIGHT, J. A. 2006. Controls on the basinwide architecture of late Miocene (Messinian) evaporites on the Levant margin (Eastern Mediterranean). *Sedimentary Geology,* 188**,** 93-114.

BERTONI, C. & CARTWRIGHT, J. A. 2007. Major erosion at the end of the Messinian Salinity Crisis: evidence from the Levant Basin, Eastern Mediterranean. *Basin Research,* 19**,** 1-18.

BROWN, A. R., BROWN, A. R., BROWN, A. R. & BROWN, A. R. 2004. *Interpretation of three-dimensional seismic data*, American Association of Petroleum Geologists Tulsa.

BROWN, K. & WESTBROOK, G. 1988. Mud diapirism and subcretion in the Barbados Ridge accretionary complex: the role of fluids in accretionary processes. *Tectonics,* 7**,** 613-640.

BROWN, K. M. 1990. The nature and hydrogeologic significance of mud diapirs and diatremes for accretionary systems. *Journal of Geophysical Research,* 95**,** 8969-8982.

CALVES, G., SCHWAB, A., HUUSE, M., VAN RENSBERGEN, P., CLIFT, P., TABREZ, A. & INAM, A. 2010. Cenozoic mud volcano activity along the Indus Fan: offshore Pakistan. *Basin Research,* 22**,** 398-413.

CARTWRIGHT, J. & SANTAMARINA, C. 2015. Seismic characteristics of fluid escape pipes in sedimentary basins: implications for pipe genesis. *Marine and Petroleum Geology*.

CARTWRIGHT, J. A. & JACKSON, M. P. A. 2008. Initiation of gravitational collapse of an evaporite basin margin: The Messinian saline giant, Levant Basin, eastern Mediterranean. *Geological Society of America Bulletin,* 120**,** 399-413.

CIESM 2008. The Messinian Salinity Crisis from mega-deposits to microbiology - A consensus report. *N° 33 in CIESM Workshop Monographs [F. Briand, Ed.], 168 pages, Monaco.*

DIMITROV, L. I. 2002. Mud volcanoes--the most important pathway for degassing deeply buried sediments. *Earth-Science Reviews,* 59**,** 49-76.

DOLSON, J., BOUCHER, P., SIOK, J. & HEPPARD, P. Key challenges to realizing full potential in an emerging giant gas province: Nile Delta/Mediterranean offshore, deep water, Egypt. Geological Society, London, Petroleum Geology Conference series, 2005. Geological Society of London, 607-624.

DOLSON, J., SHANN, M., MATBOULY, S., HAMMOUDA, H. & RASHED, R. 2001. Egypt in the twenty-first century: petroleum potential in offshore trends. *GEOARABIA-MANAMA-,* 6**,** 211-230.

DOWNEY, M. W. 1984. Evaluating seals for hydrocarbon accumulations. *AAPG Bulletin,* 68**,** 1752-1763.

DUGGEN, S., HOERNLE, K., VAN DEN BOGAARD, P., RÜPKE, L. & MORGAN, J. P. 2003. Deep roots of the Messinian salinity crisis. *Nature,* 422**,** 602-606.

DUPRÉ, S., MASCLE, J., FOUCHER, J.-P., HARMEGNIES, F., WOODSIDE, J. & PIERRE, C. 2014. Warm brine lakes in craters of active mud volcanoes, Menes caldera off NW Egypt: evidence for deep-rooted thermogenic processes. *Geo-Marine Letters,* 34**,** 153-168.

DUPRE, S., WOODSIDE, J., FOUCHER, J.-P., DE LANGE, G., MASCLE, J., BOETIUS, A., MASTALERZ, V., STADNITSKAIA, A., ONDREAS, H., HUGUEN, C., HARMEGNIES, F. O., GONTHARET, S., LONCKE, L., DEVILLE, E., NIEMANN, H., OMOREGIE, E., ROY, K. O.-L., FIALA-MEDIONI, A., DAHLMANN, A., CAPRAIS, J.-C., PRINZHOFER, A., SIBUET, M., PIERRE, C., DAMSTE, J. S. S. & PARTY, N. S. 2007. Seafloor geological studies above active gas chimneys off Egypt (Central nile deep sea fan). *Deep-Sea Research Part I-Oceanographic Research Papers,* 54**,** 1146-1172.

DUPRÉ, S., WOODSIDE, J., KLAUCKE, I., MASCLE, J. & FOUCHER, J.-P. 2010. Widespread active seepage activity on the Nile Deep Sea Fan (offshore Egypt) revealed by high-definition geophysical imagery. *Marine Geology,* 275**,** 1-19.

FOWLER, S., MILDENHALL, J., ZALOVA, S., RILEY, G., ELSLEY, G., DESPLANQUES, A. & GULIYEV, F. 2000. Mud volcanoes and structural development on Shah Deniz. *Journal of Petroleum Science and Engineering,* 28**,** 189-206.

FUKUSHIMA, Y., MORI, J., HASHIMOTO, M. & KANO, Y. 2009. Subsidence associated with the LUSI mud eruption, East Java, investigated by SAR interferometry. *Marine and Petroleum Geology,* 26**,** 1740-1750.

GAULLIER, V., MART, Y., BELLAICHE, G., MASCLE, J., VENDEVILLE, B. C., ZITTER, T. & PARTY, S. L. P. I. I. S. 2000. Salt tectonics in and around the Nile deep-sea fan: insights from the PRISMED II cruise. *Geological Society, London, Special Publications,* 174**,** 111-129.

GIRESSE, P., LONCKE, L., HUGUEN, C., MULLER, C. & MASCLE, J. 2010. Nature and origin of sedimentary clasts associated with mud volcanoes in the Nile deep-sea fan. Relationships with fluid venting. *Sedimentary Geology,* 228**,** 229-245.

GRASSO, M., LENTINI, F. & PEDLEY, H. 1982. Late tortonian—lower messinian (miocene) palaeogeography of SE Sicily: information from two new formations of the sorting group. *Sedimentary Geology,* 32**,** 279-300.

HERMANRUD, C., VENSTAD, J. M., CARTWRIGHT, J., RENNAN, L., HERMANRUD, K. & BOLÅS, H. M. N. 2013. Consequences of water level drops for soft sediment deformation and vertical fluid leakage. *Mathematical Geosciences,* 45**,** 1-30.

HIRSCH, F., FLEXER, A., ROSENFELD, A. & YELLINDROR, A. 1995. Palinspastic and crustal setting of the Eastern Mediterranean. *Journal of Petroleum Geology,* 18**,** 149-170.

HSÜ, K. J., MONTADERT, L., BERNOULLI, D., CITA, M. B., GARRISON, R. E., KIDD, R. B., MELIERES, F., MÜLLER, C. & WRIGHT, R. 1977. History of the Mediterranean salinity crisis. *Structural history of the Mediterranean basins***,** 421.

HUDEC, M. R. & JACKSON, M. 2007. Terra infirma: Understanding salt tectonics. *Earth-Science Reviews,* 82**,** 1-28.

HUGUEN, C., FOUCHER, J. P., MASCLE, J., ONDREAS, H., THOUEMENT, M., GONTHARET, S., STADNITSKAIA, A., PIERRE, C., BAYON, G. & LONCKE, L. 2009. Menes caldera, a highly active site of brine seepage in the Eastern Mediterranean sea:" In situ" observations from the NAUTINIL expedition (2003). *Marine Geology,* 261**,** 138-152.

HUGUEN, C., MASCLE, J., CHAUMILLON, E., KOPF, A., WOODSIDE, J. & ZITTER, T. 2004. Structural setting and tectonic control of mud volcanoes from the Central Mediterranean Ridge (Eastern Mediterranean). *Marine Geology,* 209**,** 245-263.

IMBERT, P., GEISS, B. & DE MARTÍN, N. F. 2014. How to evacuate 10 km3 of mud: saturate with gas and decrease the pressure! *Geo-Marine Letters,* 34**,** 199-213.

ISTADI, B. P., PRAMONO, G. H., SUMINTADIREJA, P. & ALAM, S. 2009. Modeling study of growth and potential geohazard for LUSI mud volcano: East Java, Indonesia. *Marine and Petroleum Geology,* 26**,** 1724-1739.

JAKUBOV, A., ALI-ZADE, A. & ZEINALOV, M. 1971. Atlas of Mud Volcanoes in the Azerbaijan SSR. *Azerbaijan Academy of Sciences, Baku, Azerbaijan*.

JUDD, A. G. & HOVLAND, M. 2007. *Seabed fluid flow: the impact of geology, biology and the marine environment*, Cambridge University Press.

KHOLODOV, V. 2002. Mud volcanoes, their distribution regularities and genesis: communication 1. Mud volcanic provinces and morphology of mud volcanoes. *Lithology and Mineral Resources,* 37**,** 197-209.

KOPF, A. & BEHRMANN, J. H. 2000. Extrusion dynamics of mud volcanoes on the Mediterranean Ridge accretionary complex. *Geological Society, London, Special Publications,* 174**,** 169-204.

KOPF, A., KLAESCHEN, D. & MASCLE, J. 2001. Extreme efficiency of mud volcanism in dewatering accretionary prisms. *Earth and Planetary Science Letters,* 189**,** 295-313.

KOPF, A. J. 2002. Significance of mud volcanism. *Reviews of Geophysics,* 40**,** 1-52.

LAWRENCE, G. W. & CARTWRIGHT, J. A. 2010. The stratigraphic and geographic distribution of giant craters and remobilised sediment mounds on the mid Norway margin, and their relation to long term fluid flow. *Marine and Petroleum Geology,* 27**,** 733-747.

LONCKE, L., GAULLIER, V., MASCLE, J., VENDEVILLE, B. & CAMERA, L. 2006. The Nile deep-sea fan: an example of interacting sedimentation, salt tectonics, and inherited subsalt paleotopographic features. *Marine and Petroleum Geology,* 23**,** 297-315.

LONCKE, L., MASCLE, J. & PARTIES, F. S. 2004. Mud volcanoes, gas chimneys, pockmarks and mounds in the Nile deep-sea fan (Eastern Mediterranean): geophysical evidences. *Marine and Petroleum Geology,* 21**,** 669-689.

LORENZ, V. 1975. Formation of phreatomagmatic maar-diatreme volcanoes and its relevance to kimberlite diatremes. *Physics and Chemistry of the Earth,* 9**,** 17-27.

LOWE, D. R. 1975. Water escape structures in coarse-grained sediments. *Sedimentology,* 22**,** 157-204.

MAGARA, K. 1978. *Compaction and fluid migration*, Elsevier.

MASCLE, J., BENKHELIL, J., BELLAICHE, G., ZITTER, T., WOODSIDE, J., LONCKE, L. & PARTY, P. I. I. S. 2000. Marine geologic evidence for a Levantine-Sinai plate, a new piece of the Mediterranean puzzle. *Geology,* 28**,** 779-782.

MASCLE, J., MARY, F., PRAEG, D., BROSOLO, L., CAMERA, L., CERAMICOLA, S. & DUPRÉ, S. 2014. Distribution and geological control of mud volcanoes and other fluid/free gas seepage features in the Mediterranean Sea and nearby Gulf of Cadiz. *Geo-Marine Letters,* 34**,** 89-110.

MASCLE, J., SARDOU, O., LONCKE, L., MIGEON, S., CAMÉRA, L. & GAULLIER, V. 2006. Morphostructure of the Egyptian continental margin: insights from swath bathymetry surveys. *Marine Geophysical Researches,* 27**,** 49-59.

MAZZINI, A., ETIOPE, G. & SVENSEN, H. 2012. A new hydrothermal scenario for the 2006 Lusi eruption, Indonesia. Insights from gas geochemistry. *Earth and Planetary Science Letters,* 317**,** 305-318.

MAZZINI, A., NERMOEN, A., KROTKIEWSKI, M., PODLADCHIKOV, Y., PLANKE, S. & SVENSEN, H. 2009. Strike-slip faulting as a trigger mechanism for overpressure release through piercement structures. Implications for the Lusi mud volcano, Indonesia. *Marine and Petroleum Geology,* 26**,** 1751-1765.

MAZZINI, A., SVENSEN, H., AKHMANOV, G., ALOISI, G., PLANKE, S., MALTHE-SØRENSSEN, A. & ISTADI, B. 2007. Triggering and dynamic evolution of the LUSI mud volcano, Indonesia. *Earth and Planetary Science Letters,* 261**,** 375-388.

MCCLUSKY, S., BALASSANIAN, S., BARKA, A., DEMIR, C., ERGINTAV, S., GEORGIEV, I., GURKAN, O., HAMBURGER, M., HURST, K. & KAHLE, H. 2000. Global Positioning System constraints on plate kinematics and dynamics in the eastern Mediterranean and Caucasus. *Journal of Geophysical Research: Solid Earth (1978–2012),* 105**,** 5695-5719.

MCKENZIE, D. P. 1970. PLATE TECTONICS OF MEDITERRANEAN REGION. *Nature,* 226**,** 239-&.

MCKENZIE, J. A. 1999. From desert to deluge in the Mediterranean. *Nature,* 400**,** 613-613.

MILKOV, A. V. 2000. Worldwide distribution of submarine mud volcanoes and associated gas hydrates. *Marine Geology,* 167**,** 29-42.

MORELLI, C. 1978. EASTERN MEDITERRANEAN - GEOPHYSICAL RESULTS AND IMPLICATIONS. *Tectonophysics,* 46**,** 333-346.

MOSS, J., CARTWRIGHT, J., CARTWRIGHT, A. & MOORE, R. 2012. The spatial pattern and drainage cell characteristics of a pockmark field, Nile Deep Sea Fan. *Marine and Petroleum Geology,* 35**,** 321-336.

NERMOEN, A., GALLAND, O., JETTESTUEN, E., FRISTAD, K., PODLADCHIKOV, Y., SVENSEN, H. & MALTHE-SORENSSEN, A. 2010. Experimental and analytic modeling of piercement structures. *Journal of Geophysical Research-Solid Earth,* 115.

OSBORNE, M. J. & SWARBRICK, R. E. 1997. Mechanisms for generating overpressure in sedimentary basins; a reevaluation. *AAPG Bulletin,* 81**,** 1023-1041.

PIERRE, C., BAYON, G., BLANC-VALLERON, M.-M., MASCLE, J. & DUPRÉ, S. 2014. Authigenic carbonates related to active seepage of methane-rich hot brines at the Cheops mud volcano, Menes caldera (Nile deep-sea fan, eastern Mediterranean Sea). *Geo-Marine Letters,* 34**,** 253-267.

PRATHER, B. E., BOOTH, J. R., STEFFENS, G. S. & CRAIG, P. A. 1998. Classification, lithologic calibration, and stratigraphic succession of seismic facies of intraslope basins, deep-water Gulf of Mexico. *AAPG bulletin,* 82**,** 701-728.

PRINZHOFER, A. & DEVILLE, E. 2011. Origins of hydrocarbon gas seeping out from offshore mud volcanoes in the Nile delta. *Tectonophysics*.

RIIS, F., BERG, K., CARTWRIGHT, J., EIDVIN, T. & HANSCH, K. 2005. Formation of large, crater-like evacuation structures in ooze sediments in the Norwegian Sea. Possible implications for the development of the Storegga Slide. *Marine and Petroleum Geology,* 22**,** 257-273.

ROBERTSON, A. 1996. Mud volcanism on the Mediterranean Ridge: Initial results of Ocean Drilling Program Leg 160. *Geology,* 24**,** 239-242.

ROSS, D. A. & UCHUPI, E. 1977. Structure and sedimentary history of southeastern Mediterranean Sea-Nile Cone area. *American Association of Petroleum Geologists Bulletin,* 61**,** 872-902.

RYAN, W. B. & CITA, M. B. 1978. The nature and distribution of Messinian erosional surfaces—Indicators of a several-kilometer-deep Mediterranean in the Miocene. *Marine Geology,* 27**,** 193-230.

SAGE, L. & LETOUZEY, J. 1990. Convergence of the African and Eurasian plate in the eastern Mediterranean. *Petroleum and tectonics in mobile belts***,** 49-68.

SAID, R. 1962. The geology of Egypt. *New york*.

SALEM, R. 1976. Evolution of Eocene-Miocene sedimentation patterns in parts of northern Egypt. *AAPG Bulletin,* 60**,** 34-64.

SAMUEL, A., KNELLER, B., RASLAN, S., SHARP, A. & PARSONS, C. 2003. Prolific deep-marine slope channels of the Nile Delta, Egypt. *AAPG bulletin,* 87**,** 541-560.

STEWART, S. A. & DAVIES, R. J. 2006. Structure and emplacement of mud volcano systems in the South Caspian Basin. *AAPG bulletin,* 90**,** 771-786.

TANIKAWA, W., SAKAGUCHI, M., WIBOWO, H. T., SHIMAMOTO, T. & TADAI, O. 2010. Fluid transport properties and estimation of overpressure at the Lusi mud volcano, East Java Basin. *Engineering Geology,* 116**,** 73-85.

TERZAGHI, K., TERZAGHI, K., ENGINEER, C., CZECHOSLOWAKIA, A., TERZAGHI, K., CIVIL, I., TCHÉCOSLOVAQUIE, A. & UNIS, E. 1951. *Mechanism of landslides*, Harvard University, Department of Engineering.

VANDRÉ, C., CRAMER, B., GERLING, P. & WINSEMANN, J. 2007. Natural gas formation in the western Nile delta (Eastern Mediterranean): thermogenic versus microbial. *Organic Geochemistry,* 38**,** 523-539.

YAKUBOV, A., ALI-ZADE, A. & ZEILANOV, M. 1971. Mud volcanoes of Azerbaijan. *SSR: Atlas, Azerbaijan Academy of Science, Baku*.

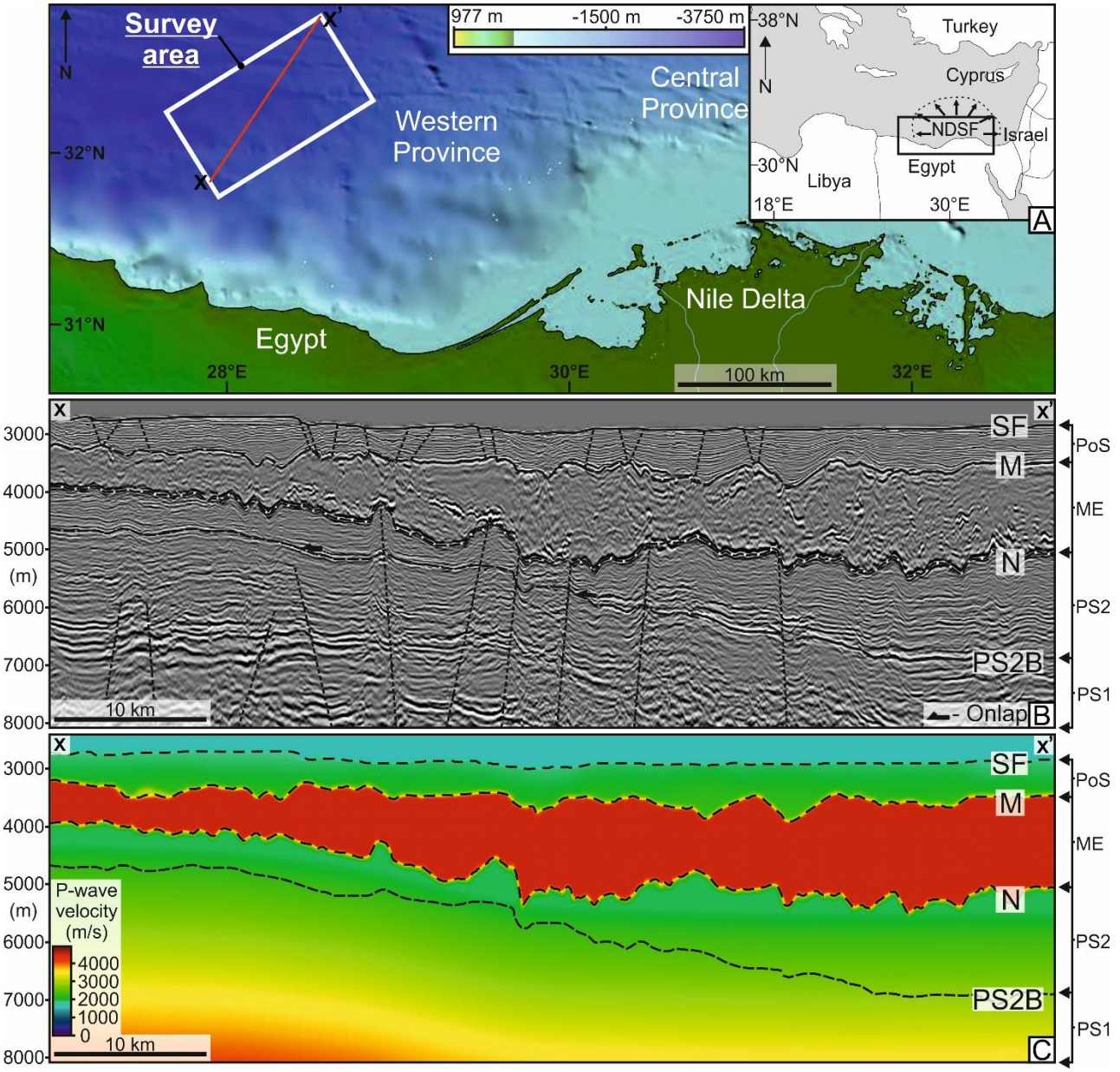

Figure 1. A: Location map of the study area in the western province, Eastern Mediterranean, showing the setting of the three-dimensional (3D) seismic survey used in this study (white box) and the line of section for Fig. 1B and Fig. 1C (red line x-x'). The dashed black line within the regional Eastern Mediterranean map displays the approximate margins of the Nile Deep Sea Fan (NDSF). B: Pre-stack depth migrated seismic profile through the study area showing the main stratigraphic units. C: Pre-stack depth migrated velocity profile displaying p-wave velocity throughout the successions within this study area. SF – Seafloor; M – Horizon M; N – Horizon N; PS2B – Pre-salt 2 base; PoS – Post-salt; ME – Messinian Evaporites; PS1 – Pre-salt 1; PS2 - Pre-salt 2.

(2 column fitting image)

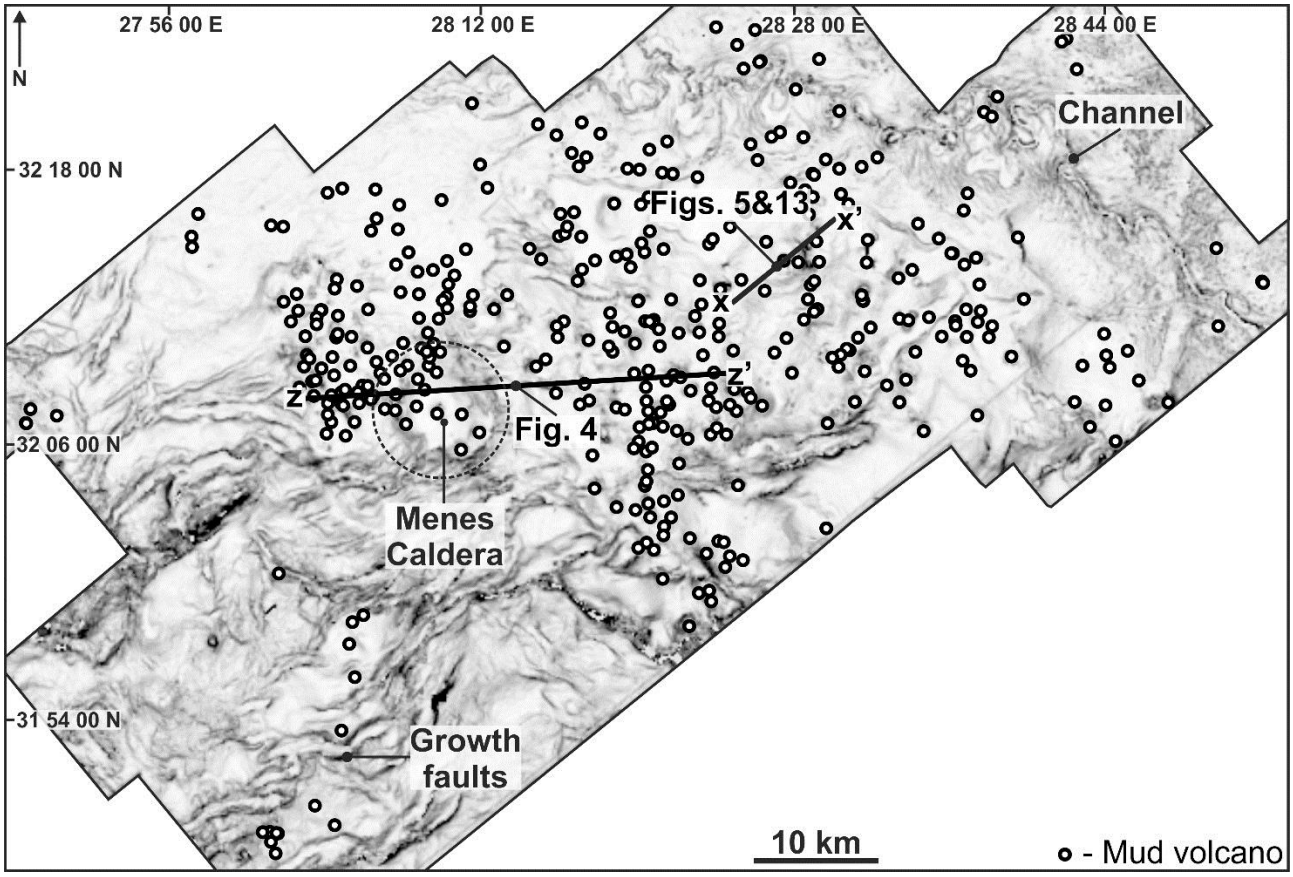

Figure 2. A Seafloor dip map within the seismic study area showing the location of all 386 mud volcanoes within the post-salt succession (white points), the majority of which are concentrate in the central region of the study area. Highlighted on the map are prominent modern seafloor features including growth faults within the SW of the study area, a channel levee complex to the NE and the c. 8 km wide seafloor depression of the Menes Caldera. The line of seismic section in Fig. 4 (z-z'), and Fig. 5 and Fig. 13 (x-x') is displayed.

(2 column fitting image)

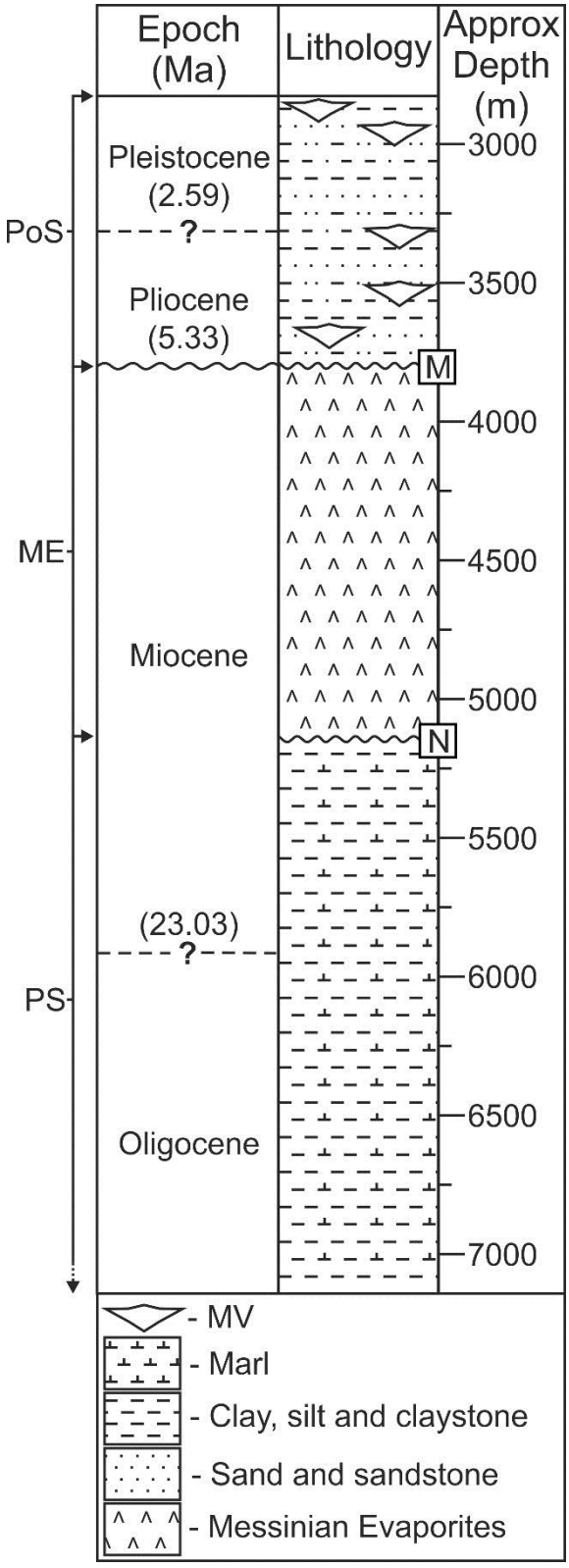

Figure 3. Stratigraphic chart showing the main sedimentary successions within this study area. Due to a lack of well calibration within the immediate area, this interpretation is based on 3D seismic observations and stratigraphic charts further to the west within the Levant basin (Modified from Bertoni and Cartwright (2005)). M – Horizon M; N – Horizon N; PoS – Post-salt; ME – Messinian Evaporites; PS – Pre-salt.

(1 column fitting image)

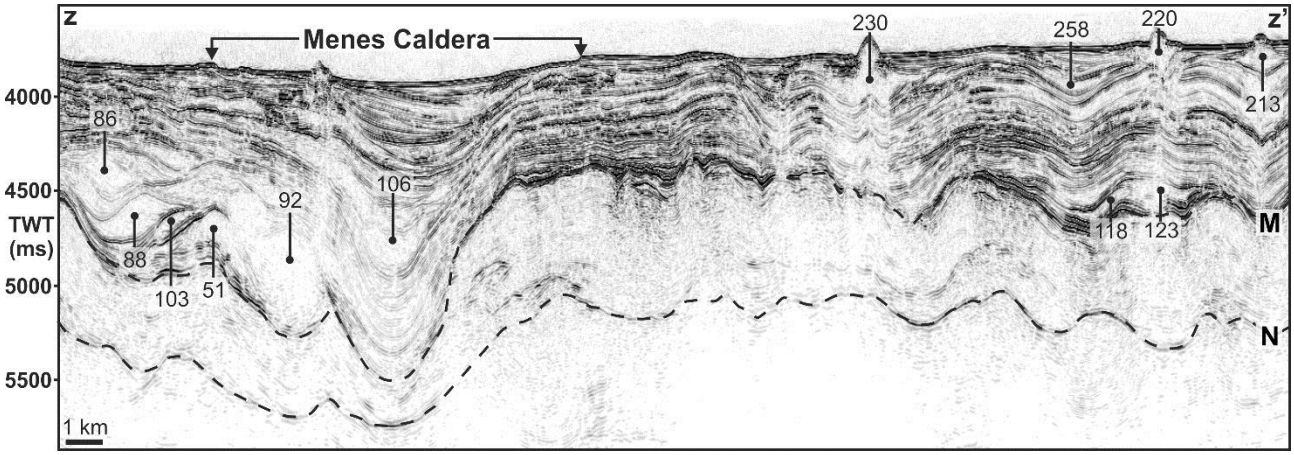

Figure 4. Pre-stack time migrated seismic profile displaying numerous mud volcanoes throughout the post-salt succession within this study area. The mud volcanoes exhibit lensoid and conical geometry and are annotated based on their ID number. Mud volcanoes buried more deeply within the post-salt succession such as mud volcanoes number 118 and 123 exhibit a deformed geometry. The seismic profile also shows the Menes Caldera which is characterised by a seafloor depression, beneath which numerous mud volcanoes are located. M – Horizon M; N – Horizon N. The line of section is displayed in Fig. 2.

(2 column fitting image)

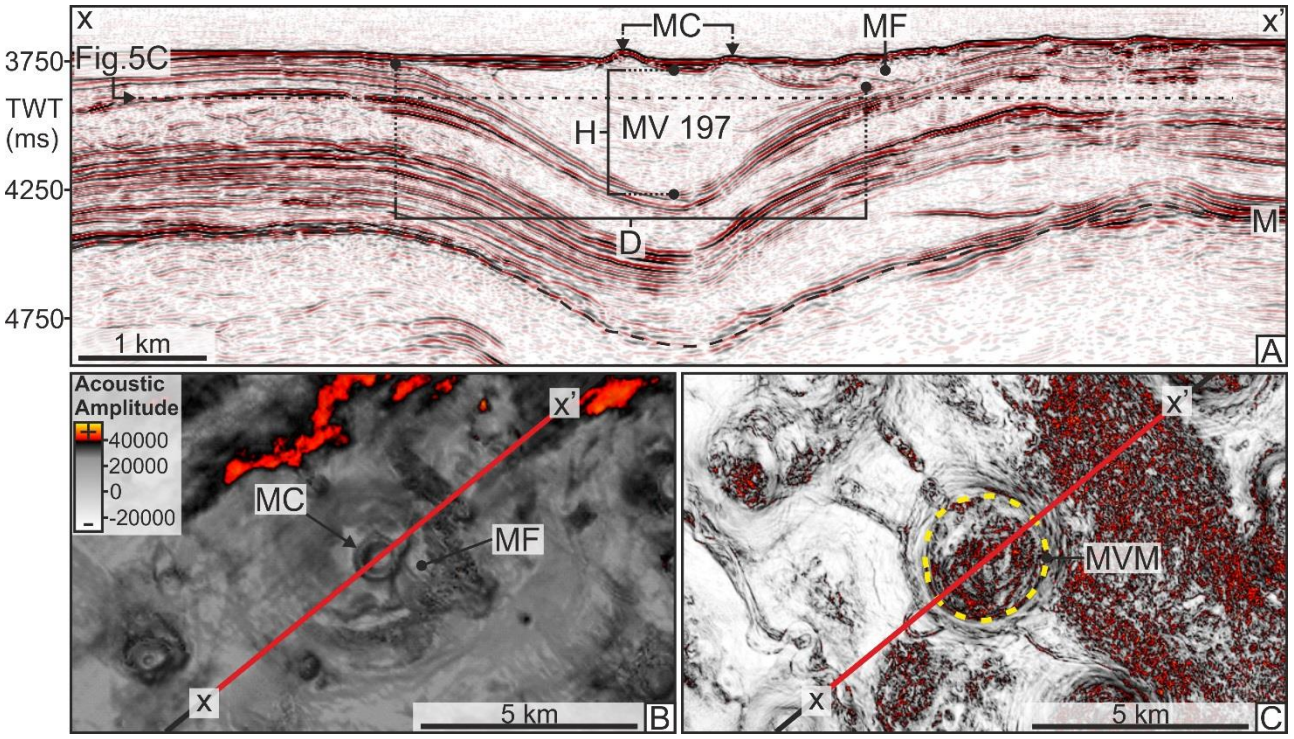

Figure 5 A: Pre-stack time migrated seismic profile through mud volcano 197. The mud volcano is thickest at its centre and thins towards its flanks and displays an overall conical geometry. The hemipelagic deposits and reflection of Horizon M (M) that underlie the mud volcano display a concave upward geometry that is concordant with the basal surface of the mud volcano. The height (H) of the mud volcano is measured as the distance from the basal surface of the mud volcano to its upper surface, through its centrally thickest region. The diameter (D) is measured as the distance through the centre of the mud volcano from one lateral margin, where the upper and basal surfaces converge, to the other. A mud flow (MF) adjacent to the mud cone (MV) at the upper surface can also be seen. The line of section can be seen in Fig. 2. B: An amplitude dip map of the seafloor displaying the mud cone of MV 197 and the mud flow also visible in the seismic profile in Fig. 5A. C: Horizontal variance slice through MV 197 that clearly displays a circular to sub-circular areas of discontinuity with abrupt margins (yellow dashed line). MVM – Mud volcano margins.

(2 column fitting image)

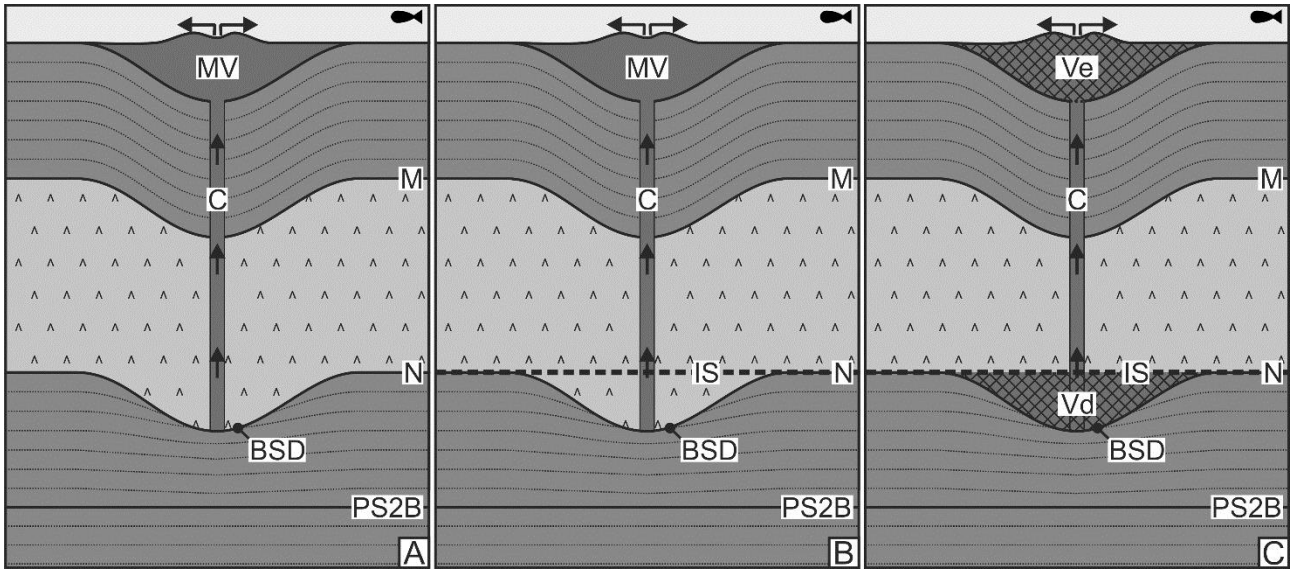

Figure 6 A: A schematic of a mud volcano at the seafloor with an underlying base-salt depression (BSD). B: A similar schematic to the one in Fig. 6A, but with an interpolated surface (IS) that forms the best fit to the relief of the region immediately surrounding the base salt depression. The volume between Sub-Unit PS2's base (PS2B) and Horizon N (N), and the volume between PS2B and IS, can be calculated C: A schematic displaying the volume balance between a depletion zone and mud volcano. The calculated volume between PS2B and BSD can be subtracted from the volume calculated between PS2B and IS, to give the volume within the depression referred to as the depletion volume (Vd). The volume of mud within the extruded mud volcano is referred to as the extruded volume (Ve). The depletion volume was remobilised and extruded at the seafloor as a mud volcano, therefore the depletion volume is approximately equal to the extruded volume (Vd≈Ve). The arrows represent the migrating mud slurry. M – Horizon M; MV – Mud volcano; C – Conduit.

(2 column fitting image)

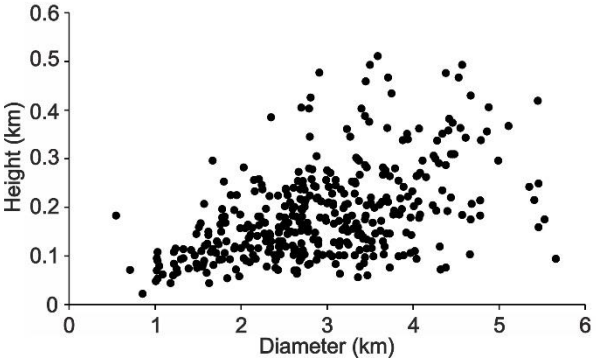

Figure 7 A plot of mud volcano height vs diameter.

(1 column fitting image)

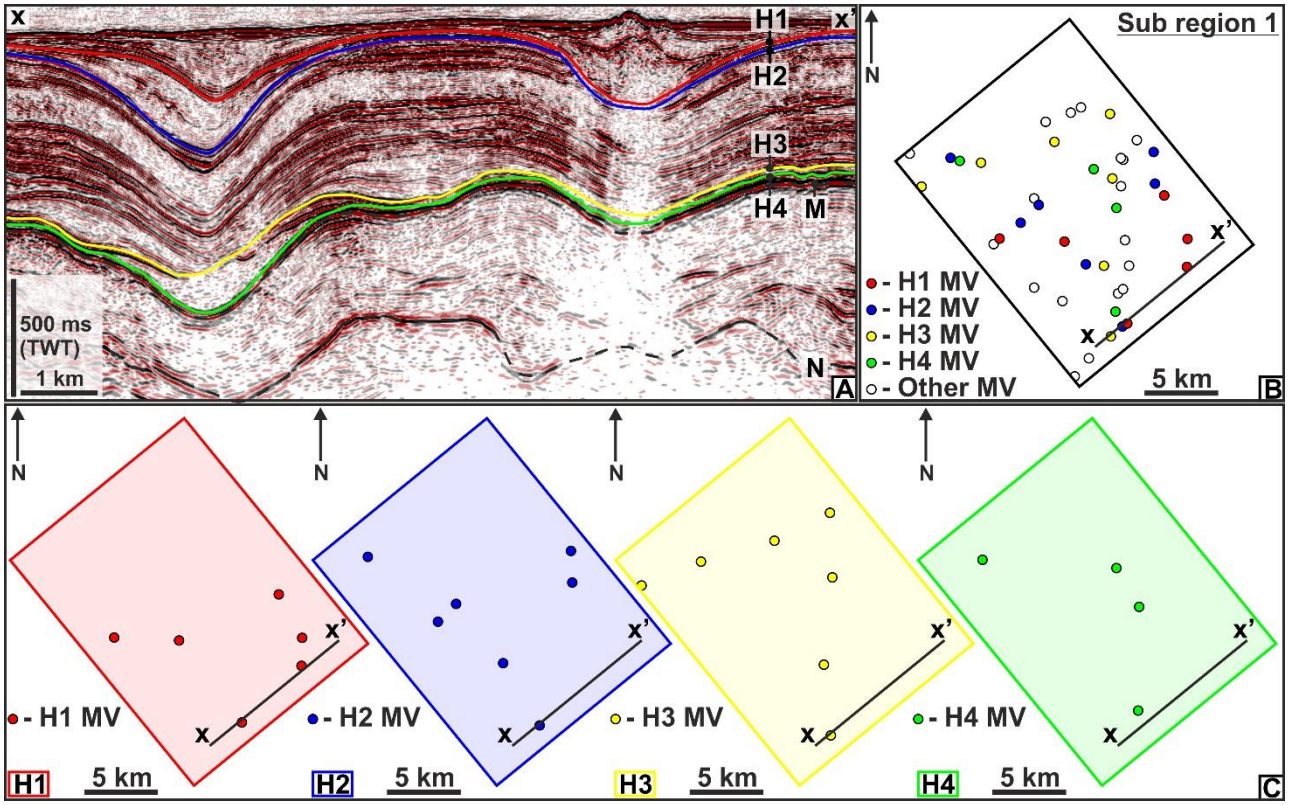

Figure 8. A) Seismic profile through sub region 1 (SR1), the line of section of which is displayed in Fig. 6B. Numerous mud volcanoes are displayed along various reflections. Mapped reflections include Horizon 1 (H1) (Red line), Horizon 2 (H2) (Blue line), Horizon 3 (H3) (Yellow line) and Horizon 4 (H4) (Green line) reflection. M – Horizon M; N – Horizon N. B) Outline of SR1 showing the location of all mud volcanoes. Mud volcanoes are colour coded depending on whether they are located along H1, H2, H3, and H4, or other. See Fig. 10B for location of SR1. C) Outline maps of SR1 colour coded based on the mapped reflections of H1 (red), H2 (blue), H3 (yellow) and H4 (green) showing the location of mud volcanoes along those Horizons. MV – Mud volcano.

(2 column fitting image)

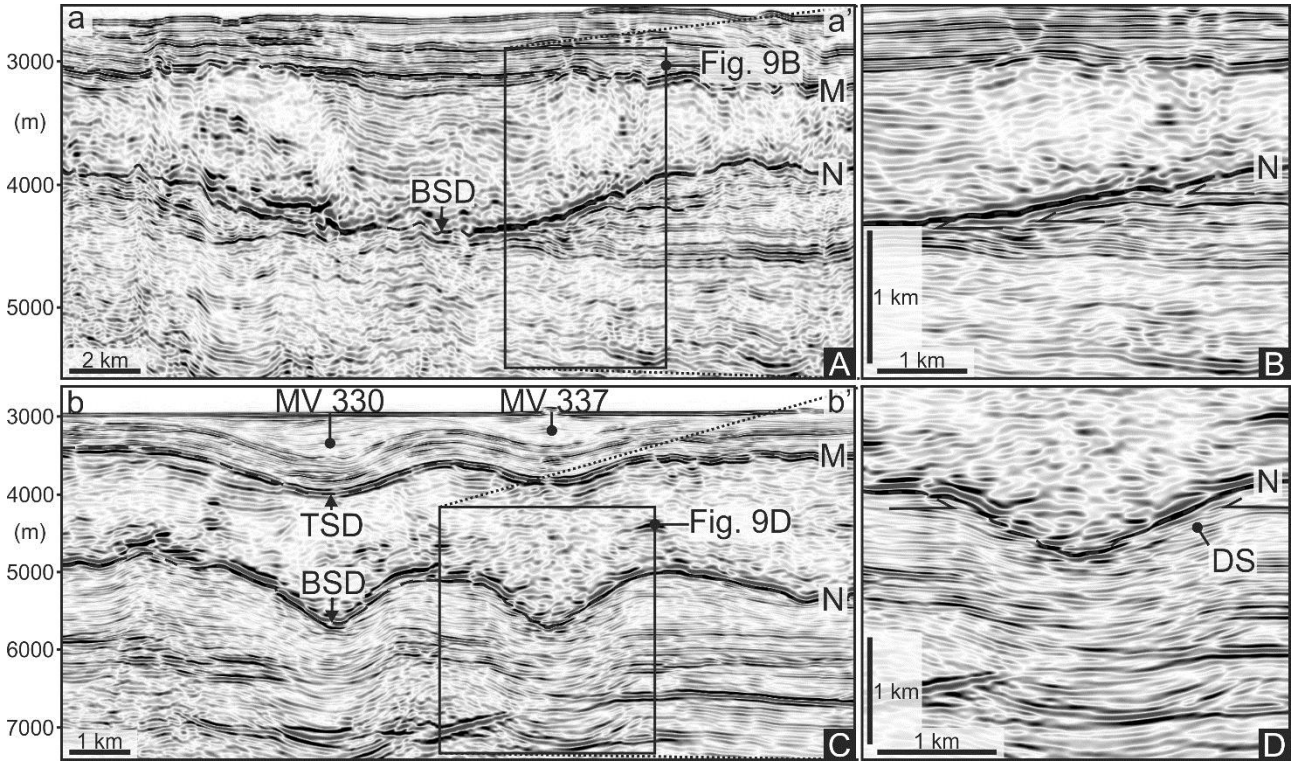

Figure 9. A: Pre-stack depth migrated seismic profile that displays a depression at Horizon N (N) and angular erosional truncation of the reflections of Sub-Unit PS2 by Horizon N. The top-salt relfection of Horizon M (M) is discordant with Horizon N and the evaporite succession increase in thickness within the depression, and no mud volcano overly this base-salt depression. B: A zoomed window of part of the seismic profile in Fig. 9A, that clearly shows the erosional truncation of Sub-Unit PS2 reflections by Horizon N. C: Pre-stack depth migrated seismic profile showing two depressions at Horizon N and concordant depression at Horizon M (M), both of which are overlain by mud volcanoes (MV). The stratal geometries of the reflections of Sub-Unit PS2 and Horizon N are unclear along margin of the depressions. Reflections display a change in angle and some concordance with Horizon N. D: A zoomed window of one of the depression in Fig. 9C, providing a clearer view of the stratal geometries. BSD – Base-salt depression; TSD – Top-salt depression; DS - Downsagging.

(2 column fitting image)

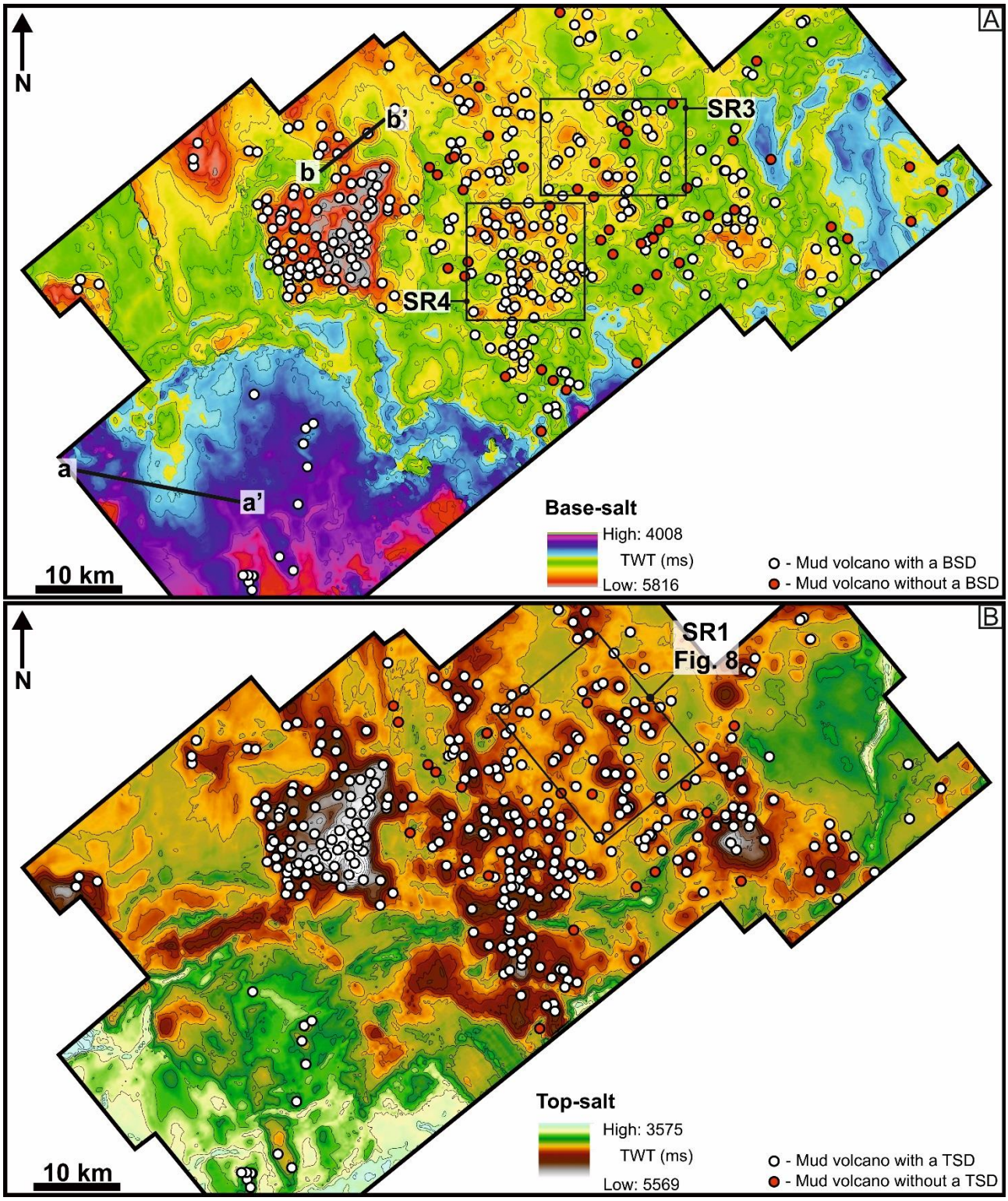

Figure 10. A: Contoured base-salt (Horizon N) time map also showing the mud volcanoes that overly a base-salt depression (BSD) (338 mud volcanoes) and those that do not (48 mud volcanoes. The location of sub region 1 (SR3) and sub region 2 (SR4) and lines of section for Fig. 9A (a-a') and Fig. 9C (b-b') are displayed. B: Contoured top-salt (Horizon M) time map and mud volcanoes that overly a base-salt depression (TSD) (365 mud volcanoes) and those that do not (21 mud volcanoes).

(2 column fitting image)

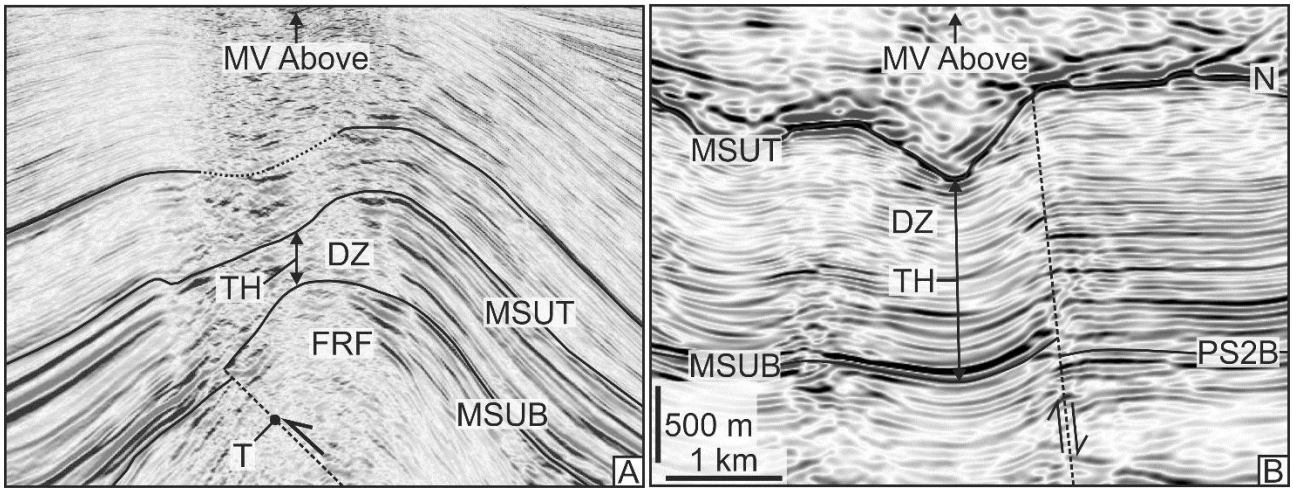

Figure 11 A: A modified seismic profile of a depletion zone (DZ) from Stewart and Davies (2006), which displays a fault related fold (FRF) and significant thinning (TH) of the source unit that underlies a mud volcano (MV). B: A pre-stack depth migrated seismic profile through a depletion zone underlying a mud volcano within this study area. This example is comparable to the example in Fig. 11A in that the source unit thins in the region that underlies the mud volcano. MSUT – Mud source unit top; MSUB – Mud source unit base; T – Thrust; N – Horizon N; PS2B – Sub-Unit PS2 base.

(2 column fitting image)

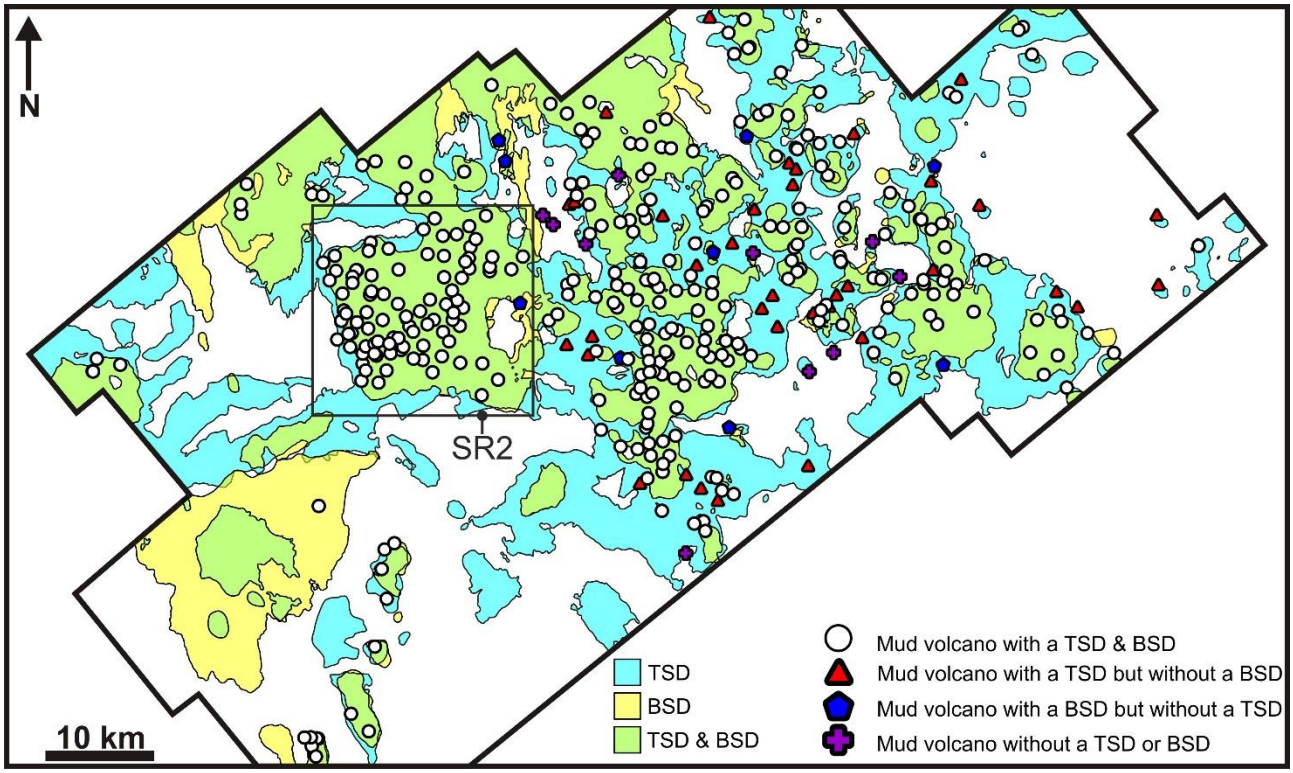

Figure 12. Map showing the outlined margins all base-salt depressions (BSD) (Yellow) and top-salt depressions (TSD) (Blue) within this study area. There is a strong spatial relationship between overlapping TSD and BSD (Green) and overlying mud volcanoes. 327 mud volcanoes overly a combined TSD and BSD; 38 mud volcanoes overly a TSD but not BSD; 11 mud volcanoes overly a BSD but without a TSD; 10 mud volcanoes do not overlie either a TSD or BSD. SR2 – Sub region 2.

(2 column fitting image)

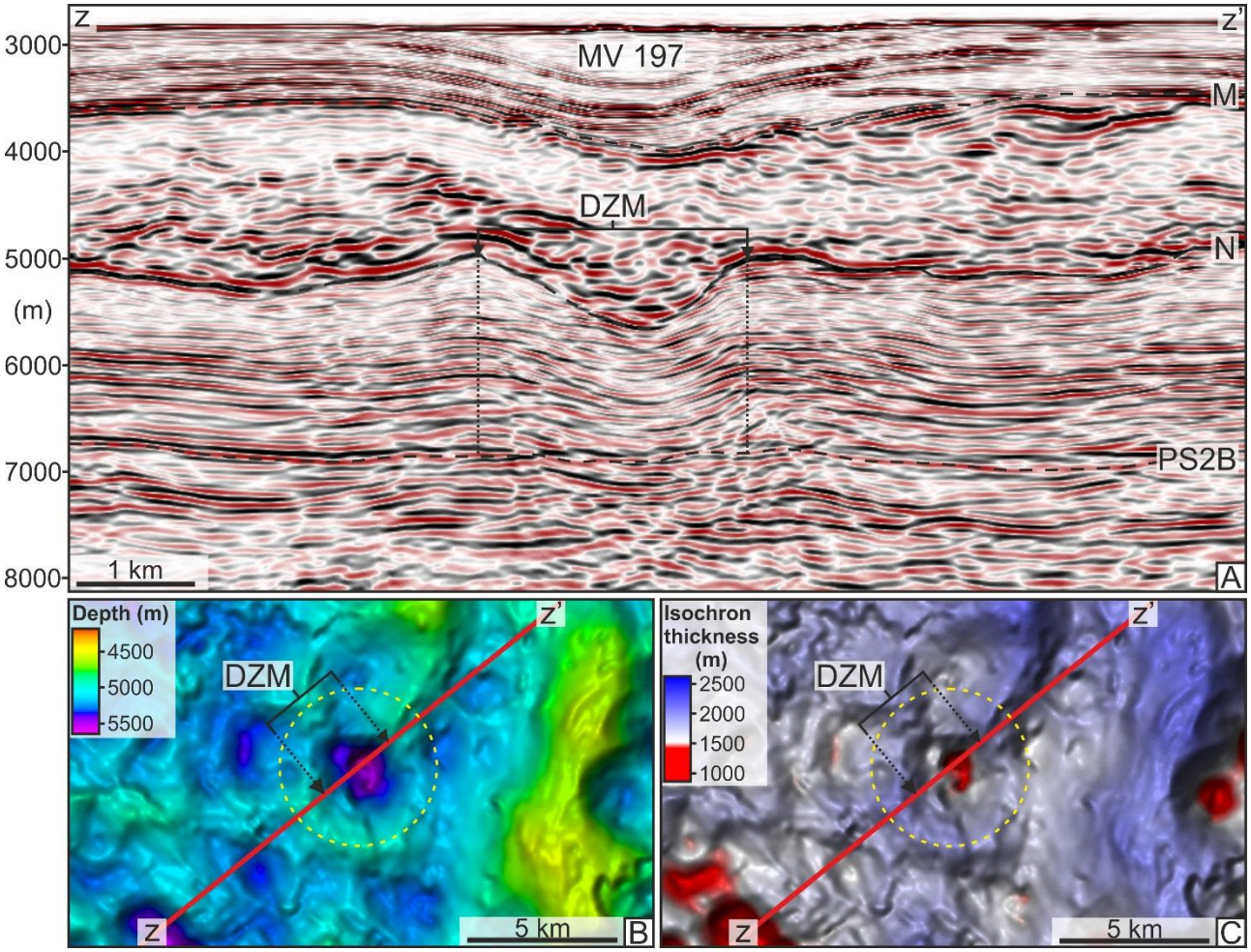

Figure 13 A: Pre-stack depth migrated seismic profile throught a mud volcano (No. 197) beneath which refelctions of the post-salt succession, Horizon M (M) and Horizon N (N) display a concave upward geometry. The line of section is the same as in Fig. 5. B: A time map of Horizon N showing a localised circular to sub-circular depression directly beneath mud volcano 197. C: A isopach map of Sub-Unit PS2 that displays anomalous and circular to sub-circular thinning of the pre-salt unit, which is spatially correlatable with the base-salt depression displayed in Fig. 13B and the overlying mud volcano seen in Fig. 13A which directly overlies. DZM – Depletion zone margins.
(2 column fitting image)

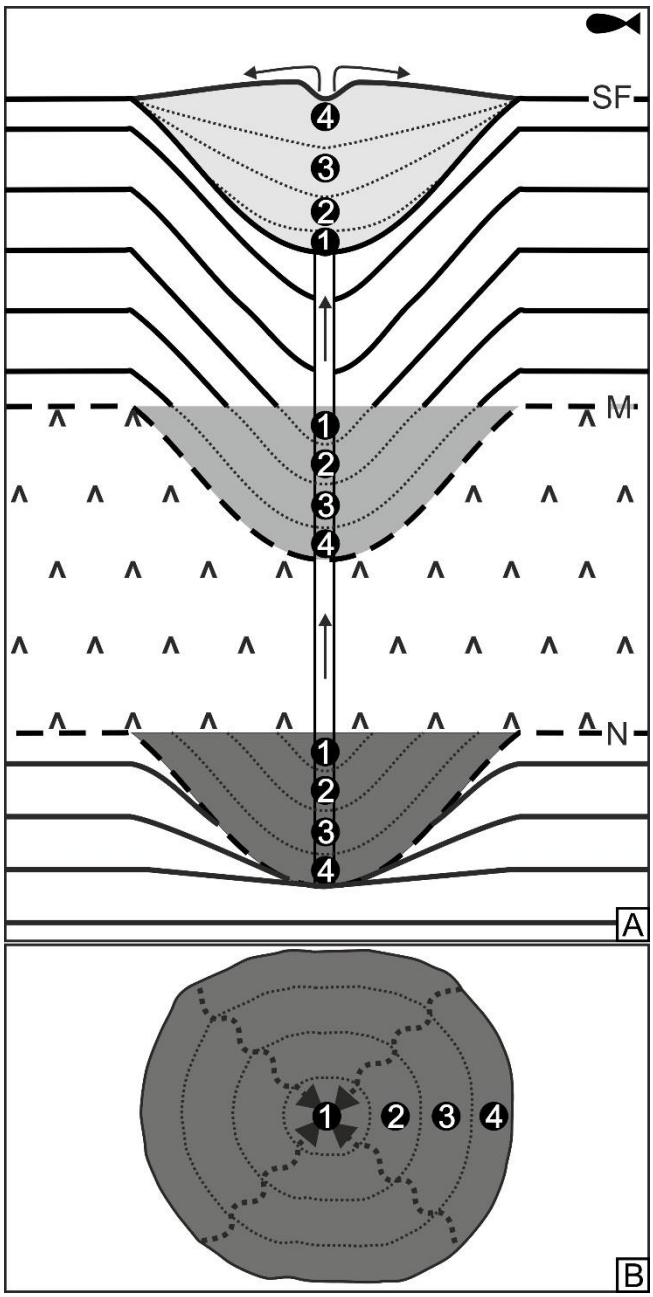

Figure 14. Conceptual model for a dynamic liquefaction process. A: A schematic representation of the various stages of a dynamic liquefaction process, represented in this example by four episodes of liquefaction and mobilisation numbered 1-4. The liquefaction and mobilisation of a volume of mud (i.e. episode 1) results in the extrusion of that volume at the seafloor and subsidence and collapse of the overburden, triggering deformation induced liquefaction and mobilisation of next episode of extrusion (i.e. episode 2), and so on for subsequent episodes. SF – Seafloor; M – Horizon M; N – Horizon N. B: A planform schematic of a concentric liquefaction and depletion zone that propagates radially outwards. Arrows represent mud and fluid mobilisation.

(1 column fitting image)